

# Photosphere-Internal Shock Model of Gamma-Ray Bursts: Case Studies of *Fermi*/LAT Bursts

K. Toma<sup>1,2</sup>, X.-F. Wu<sup>1,2,3</sup>, and P. Mészáros<sup>1,2,4</sup>  $\star$

<sup>1</sup>*Department of Astronomy and Astrophysics, Pennsylvania State University, 525 Davey Lab, University Park, PA 16802, USA*

<sup>2</sup>*Center for Particle Astrophysics, Pennsylvania State University*

<sup>3</sup>*Purple Mountain Observatory, Chinese Academy of Sciences, Nanjing 210008, China*

<sup>4</sup>*Department of Physics, Pennsylvania State University*

7 November 2018

## ABSTRACT

Radially inhomogeneous gamma-ray burst (GRB) jets release variable photospheric emission and can have internal shocks occurring above the photosphere. We generically formulate a photospheric emission model of GRBs including Compton up-scattered photospheric (UP) emission off the electrons (and positrons) in the internal shocks, and find that the photospheric emission may correspond to the traditional (Band) component at  $\lesssim 1$  MeV and the UP emission to the high-energy emission observed by *Fermi*/LAT for some GRBs at  $\gtrsim 10$  MeV. The two components can be separate in the spectrum in some cases or can mimic a smooth broad Band spectrum in other cases. We apply our formulation to the well-studied long and short LAT GRBs, GRB 080916C, GRB 090902B, and GRB 090510, and typically find reasonable parameters for fitting the time-binned spectra, although fine tuning of several parameters is required. The observed delays of the high-energy emission with respect to the MeV emission which are large compared to the variability times are unlikely to be due to simple kinematic effects of a non-evolving jet. These delays may instead be attributed to the temporal evolution of the physical parameters of the jet, and thus the delay timescales could provide a potential tool for investigating the structures of GRB jets themselves and their progenitors. The difference of the delay timescales of long and short GRBs inferred from the *Fermi* data might be due to the differences in the progenitors of long and short GRBs. Some other properties and consequences of this model are discussed, including temporal correlations among the prompt optical, the soft X-ray, and the distinct high-energy component as well as the Band component.

**Key words:** gamma ray: bursts; radiation mechanisms: non-thermal

## 1 INTRODUCTION

The origin of gamma-ray burst (GRB) prompt emission remains unclear. It has been mainly observed in the energy range of 10 keV – 1 MeV, and most of the spectra are fitted by a simple broken power-law function (so-called Band function) or a cutoff power-law function (Preece et al. 2000; Ghirlanda et al. 2002; Kaneko et al. 2006), the light curves being typically very variable. Many models have been proposed to explain these properties. Most of them invoke a relativistic jet that is energized by a newly born compact object. Currently three types of emission mechanisms in the relativistic jet are being actively discussed; photospheric,

leptonic synchrotron, and hadronic emission models. The first models assume that the thermal energy stored in the jet can be radiated as prompt emission at the Thomson photosphere (e.g., Paczynski 1986; Goodman 1986; Thompson 1994; Mészáros & Rees 2000). Here the thermal energy in the jet can be produced by the particle and/or magnetic energy dissipation between the explosion center and the photosphere. The second and third models assume the Thomson-thin region as the prompt emission site. In the second models, the electrons (and positrons) accelerated by the shock dissipation of the kinetic energy or by the magnetic energy dissipation radiate synchrotron and synchrotron-self-Compton (SSC) emissions (e.g., Rees & Mészáros 1994; Daigne & Mochkovitch 1998; Kumar & McMahon 2008; Spruit et al. 2001; Lyutikov 2006), while in the third models the accelerated protons and secondary particles induced

$\star$  E-mail toma@astro.psu.edu (KT); xfwu@pmo.ac.cn (XFW); nmp@astro.psu.edu (PM)

by the photopion cascade process produce synchrotron and inverse Compton (IC) emissions (e.g., Vietri 1997; Böttcher & Dermer 1998; Asano et al. 2009b). Clarifying the prompt emission mechanism and the physical quantities at the emission site would help understand the nature of the relativistic jet and the compact object that energizes the jet. For other models and more general discussions, see recent reviews Piran (2004), Mészáros (2006), and Zhang (2007).

GRBs were only sparsely observed in the  $> 10$  MeV energy range, until the *Fermi* satellite was launched 2008 June 11. Now the GBM (8 keV – 40 MeV) and the LAT ( $\sim 20$  MeV – 300 GeV) detectors onboard *Fermi* provide extremely broad energy coverage with good temporal resolution for GRBs. The *Fermi* observations will put further constraints on the above three types of prompt emission models. During its first 1.5 yr routine operation, the LAT has detected 14 GRBs. Those are summarized in Granot (2010). Most of their spectra are fitted by a Band function even up to  $\sim 10$  GeV, while at least 3 GRBs (GRB 090510, GRB 090902B, and GRB 090926A) have additional distinct spectral component at  $\gtrsim 10$  MeV. Those additional components are fitted by single power-law function. These 3 GRBs are among the brightest GRBs detected by *Fermi*. This suggests that such a high-energy component may be very common and we can clearly detect such a distinct high-energy component only in bright LAT GRBs (Granot 2010).

*Fermi* also revealed that the high-energy emission ( $> 100$  MeV) of most LAT GRBs is delayed behind the onset of the MeV emission, and the high-energy emission of many LAT GRBs lasts longer than the MeV emission, showing power-law decays, which are typically detected until  $\sim 10^2 - 10^3$  s. The delay times in the cosmological rest frame are  $\sim 1$  s for long GRBs and  $\lesssim 0.1$  s for short bursts GRB 081024B and GRB 090510. Although some delays of the high-energy photons are just caused by the flux increases above the LAT detection threshold without a spectral change, others must clearly be attributed to the spectral changes of the Band component and/or the onset of the distinct spectral component. We note that the distinct components of the 3 GRBs are delayed.

The origins of the distinct spectral components and the onset delays in the high-energy range have been actively debated. It has been proposed that the high-energy emission can be attributed to the external shock, which is made by the interaction of the jet with the ambient medium, and the onset delays can correspond to the times for the jet decelerations (Kumar & Barniol Duran 2009; Ghisellini et al. 2010) (see also Granot & Guetta 2003; Pe’er & Waxman 2004). However, the observed high-energy emission usually has a strong variability and it often correlates with the MeV emission, which is at odds with an external shock origin. Especially for GRB 090510, whose long-lived high-energy emission can be explained by the external shock synchrotron emission together with the optical and X-ray afterglows detected from  $\sim 100$  s after the burst trigger (De Pasquale et al. 2010; Kumar & Barniol Duran 2010; Corsi et al. 2010), it is found that the high-energy emission in the prompt phase is much brighter than that produced by the same external shock (He et al. 2010). A similar conclusion has been obtained for GRB 090902B (Liu & Wang 2010). As for the internal shock models, it is not simple

to explain the LAT onset delays which are larger than the variability timescales ( $t_v$ ) by the delayed brightening of the SSC emission (Abdo et al. 2009b,c; Ackermann et al. 2010a; Corsi et al. 2010; Daigne et al. 2011). The spectral index of the distinct high-energy component different from the Band low-energy spectral index, seen in e.g., GRB 090902B, may not be explained simply either in these models. To overcome these problems, we have proposed an external inverse Compton (EIC) component (i.e., the emission produced by up-scattering the photons incident from outside the shock) in addition to the synchrotron and SSC components in the internal shock model (Toma et al. 2009b); this model, however, requires an extreme value of the microphysical parameter  $\epsilon_B \sim 10^{-5}$ , which does not seem common. Other alternative mechanisms such as hadronic emission mechanisms require huge isotropic energies (Asano et al. 2009a; Wang et al. 2009; Razzaque et al. 2010), while magnetically-dominated jets have not been explored explicitly enough for detailed comparisons with *Fermi*/LAT observational results (see Zhang & Pe’er 2009; Fan 2010; Zhang & Yan 2011).

In this paper we concentrate on a photospheric emission model. Such models have been briefly discussed for interpreting the relation of the MeV emission with the high-energy emission. In this scenario, the photosphere produces a Band emission component which peaks around  $\sim 1$  MeV, and this cannot generally produce the high-energy emission because of large opacity for  $e^\pm$  pair creation. The high-energy emission in these models may instead arise in a dissipation region at a larger radius (Gao et al. 2009; Beloborodov 2010; Ryde et al. 2010). In this paper, we substantially extend this idea and discuss its consequences in greater depth. We focus on the case in which the energy of the jet is mainly carried by photons and baryons (where magnetic field energy is subdominant), and the dissipation mechanism at large radius is internal shock. We show that in typical cases the photospheric emission is efficiently Compton scattered by the electrons in internal shocks outside the photosphere, and find that the up-scattered photospheric (UP) emission is a good candidate for the observed high-energy emission in the prompt phase. This Compton scattering is a type of the EIC scattering, which is thought to be important for the high-energy emission of blazars (e.g., Sikola et al. 1994; Dermer & Schlickeiser 1993; Brunetti 2000; Ghisellini & Tavecchio 2009), and could also be important in the internal and external shocks in GRBs (Beloborodov 2005; Wang & Mészáros 2006; Fan et al. 2008; Toma et al. 2009b; Murase et al. 2010a,b). We make a generic formulation of the spectral types of the radiation from the photosphere and the internal shock including synchrotron and SSC emission for the cases of the efficient EIC scattering, and clarify necessary conditions for the photospheric and UP components to be dominant in the energy range of 10 keV – 10 GeV, rather than synchrotron and SSC components. This formulation is applied for the well-observed LAT long and short GRBs, GRB 080916C, GRB 090902B, and GRB 090510, and we typically find reasonable parameter sets for which the data can be explained by the photospheric and UP emission. Our model fits indicate that the observed delayed onset of the LAT emission may be interpreted as the parameter evolution of the GRB jet.

The UP emission ceases at the end of the prompt MeV

(photospheric) emission, and the subsequent long-lived high-energy emission may instead be related to the external shock (e.g., De Pasquale et al. 2010; Kumar & Barniol Duran 2010; Ghisellini et al. 2010). A different origin for the prompt and late LAT emission is in fact implied by the change in its behavior across this transition (He et al. 2010; Liu & Wang 2010). In what follows, we concentrate on the prompt emission phase. We discuss the general temporal and spectral properties of the radiation from the photosphere and the internal shock of the GRB jet in Sections 2, 3, and 4, and perform the case studies of GRB 080916C, GRB 090902B, and GRB 090510 in Section 5. Some of the implications of our results are discussed in Section 6.

## 2 PHOTOSPHERIC EMISSION

We consider that the jet is accelerated by the thermal pressure, and the magnetic field energy is subdominant. We derive the luminosity and temperature of the photospheric emission from the jet and the remaining kinetic luminosity of the jet above the photosphere, which is the luminosity budget for internal shocks, according to the standard fireball model (Paczynski 1986, 1990; Shemi & Piran 1990; Mészáros et al. 1993; Mészáros & Rees 2000; Nakar et al. 2005). We assume that the jet material is optically thick and the energy is dominated by thermal radiation at the base,  $r = r_a$ , from where it expands in the roughly adiabatic condition, i.e., without strong conversion of the kinetic energy into the thermal energy affecting the adiabatic expansion dynamics (for a continuous strong dissipation case, see Rees & Mészáros 2005). The jet material may have a Lorentz factor  $\Gamma_a \geq 1$  at the base. In particular, if the GRB originates from a massive stellar collapse and the jet suffers strong dissipation of its kinetic energy due to interaction with the stellar envelope, the front portion of the jet may have  $r_a \sim 10^{10} - 10^{11}$  cm and  $\Gamma_a \sim 10 - 10^2$  (see recent numerical simulations by Morsony et al. 2007; Lazzati et al. 2009, and discussion in Section 6). In the absence of a strong dissipation the base radius may be as small as a few of Schwarzschild radius of the central compact object, so that  $r_a \sim 10^6 (M_c/M_\odot)$  cm and  $\Gamma_a \sim 1$ , where  $M_c$  is the mass of the central object.

The observer-frame temperature at the base is

$$T_a = \left( \frac{L\Gamma_a^2}{4\pi r_a^2 c a} \right)^{1/4} \simeq 2 L_{53}^{1/4} \left( \frac{r_{a,7}}{\Gamma_a} \right)^{-1/2} \text{ MeV}/k, \quad (1)$$

where  $L$  is the isotropic equivalent luminosity of the jet, and  $a \simeq 7.56 \times 10^{-15} \text{ erg cm}^{-3} \text{ K}^{-4}$  is the Stefan constant.<sup>1</sup> For general cases of GRBs, the adiabatic index of the jet material below the photosphere is found to be  $4/3$  (see below). The dynamics of the expanding jet can be summarized as  $\Gamma \propto r$  and  $T = T_a$  for  $r \leq r_s$ , and  $\Gamma = \eta$  and  $T \propto r^{-2/3}$  for  $r \geq r_s$ , where the Lorentz factor saturation radius  $r_s = r_a \eta / \Gamma_a$ . Here we have defined  $\eta \equiv L/\dot{M}c^2$ , where  $\dot{M}$  is the isotropic equivalent mass ejection rate. We see that the ratio of the radiation and baryon entropy densities  $\sim aT'^4/n'kT'$  is constant throughout the evolution

below the photosphere and is much larger than unity if  $\eta \gg kT_a/(m_p c^2) \simeq 2 \times 10^{-3} L_{53}^{1/4} (r_{a,7}/\Gamma_a)^{-1/2}$  (where  $n'$  and  $T'$  is the baryon density and fluid temperature in the comoving frame). Thus the assumption of the adiabatic index =  $4/3$  is validated.

The  $e^\pm$  pairs drop out of equilibrium at  $T' \sim 20$  keV, at a radius  $r \simeq r_p = 1 \times 10^9 L_{53}^{1/4} (r_{a,7}/\Gamma_a)^{1/2}$  cm. We consider the case in which the jet carries enough baryons to provide an electron scattering photosphere above  $r_p$  (i.e., the case of  $\eta < 5 \times 10^6 L_{53}^{1/4} (r_{a,7}/\Gamma_a)^{1/2}$ ). Then the photosphere radius  $r_{\text{ph}}$  is defined as  $\tau = \sigma_T n' r / (2\Gamma) = 1$ , where  $\sigma_T$  is the Thomson cross section and the comoving electron density is given by  $n' = L/(4\pi r^2 m_p c^3 \eta \Gamma)$ , if there is no additional  $e^\pm$  pair creation in the jet (Abramowicz et al. 1991).

If no energy dissipation takes place around the photosphere, the photons and particles are fully thermalized, typically with the comoving temperature  $T'_{\text{ph}} \sim 0.1 - 1$  keV, and then the emerging radiation from the photosphere is a blackbody with the observer-frame temperature  $T_{\text{ph}} \simeq \Gamma_{\text{ph}} T'_{\text{ph}}$  (where  $\Gamma_{\text{ph}}$  is the Lorentz factor at  $r = r_{\text{ph}}$ ). However, some energy dissipation processes are expected to occur around the photosphere, which can make the emerging radiation spectrum deviate from a blackbody. Such processes have been demonstrated convincingly by recent analytical and numerical work: Both below and above the photosphere, a fraction of the electrons can acquire high-temperature distribution ( $\gg T'_{\text{ph}}$ ), either due to internal shocks and/or interaction of a jet with stellar envelope (Eichler & Levinson 2000; Rees & Mészáros 2005; Pe'er et al. 2005; Thompson et al. 2007; Lazzati & Begelman 2010), dissipation of excited plasma waves (Ioka et al. 2007), or nuclear collisions between protons and neutrons (Beloborodov 2010), or in magnetically-dominated jets due to scattering with turbulent Alfvén waves (Thompson 1994) or heating caused by magnetic reconnection (Giannios 2006). Multiple IC scatterings of the thermal photons by mildly relativistic electrons (with  $\gamma \sim 1$ ) can create a power-law tail extending from the thermal peak, which saturates at the comoving-frame energy  $\varepsilon' \sim m_e c^2$  as the Klein-Nishina limit or by the direct Compton cooling, which is boosted to  $\varepsilon \sim 0.1 - 1$  GeV in the observer frame. The dissipation processes also can produce a relativistic electron population, which IC-scatter the photons to even higher energies, the limitation being the  $\gamma\gamma$  absorption against lower energy photons. The low-energy spectral slope of the emerging photons should not be significantly changed in such processes, i.e., the photon index  $\alpha_{\text{ph}} \simeq 1$  (Beloborodov 2010; Lazzati & Begelman 2010).

In our baryonic jet model, we assume that the dissipation of the kinetic energy is not so strong that the jet dynamics is described by the adiabatic evolution, and the temperature of the emerging photons is given by  $T_{\text{ph}}$ . This implies that the energy flux in the possible non-thermal part above  $\varepsilon_{\text{ph}}$  should be smaller than that in the main thermal part, leading to an upper limit on the photon index  $\beta_{\text{ph}}$  of the possible power-law tail. Let us simply write down the spectral shapes of the pure thermal component and the thermal plus a non-thermal tail spectrum as  $F_\varepsilon^{\text{th}} = 0.84(\varepsilon/kT_{\text{ph}})^3 / [\exp(\varepsilon/kT_{\text{ph}}) - 1]$  and  $F_\varepsilon^{\text{nth}} = (\varepsilon/\varepsilon_{\text{ph}})^2 \min[1, (\varepsilon/\varepsilon_{\text{ph}})^{\beta_{\text{ph}}-1}]$ , respectively, where  $T_{\text{ph}} = \varepsilon_{\text{ph}}/4$ , and these are normalized as  $F_\varepsilon^{\text{th}} = F_\varepsilon^{\text{nth}}$

<sup>1</sup> We adopt the notation  $Q_x = Q/10^x$  in cgs units throughout this paper.

at  $\varepsilon = \varepsilon_{\text{ph}}$ .<sup>2</sup> Then we have  $\int_0^\infty F_\varepsilon^{\text{th}} d\varepsilon = 0.84(\pi^4/60)\varepsilon_{\text{ph}}$  and  $\int_0^\infty F_\varepsilon^{\text{nth}} d\varepsilon = [(1/3) - (\beta_{\text{ph}} + 2)^{-1}]\varepsilon_{\text{ph}}$ . The condition  $\int_0^\infty F_\varepsilon^{\text{nth}} d\varepsilon < 2 \times \int_0^\infty F_\varepsilon^{\text{th}} d\varepsilon$  provides a constraint  $\beta_{\text{ph}} \lesssim -2.5$ . The value of  $\beta_{\text{ph}}$  is expected to be determined not only by the ratio of the photon to kinetic energies but also on the electron energy distribution which depends on the type of a dominant dissipation process, which we may not specify at the current stage. Hereafter we treat  $\beta_{\text{ph}}$  as a free parameter ranging within the above constraint.

In such dissipation processes copious  $e^+e^-$  pairs may be created, which increase the Thomson photosphere radius. We parameterize the number density of electrons plus positrons (which we will call ‘leptons’ hereafter) near the photosphere as  $n'_l = \mathcal{R}n'$ , where  $\mathcal{R} \geq 1$ . Typically we can have  $\mathcal{R} \sim 10 - 10^2$ , in which case the inertia is still dominated by baryons. Thus the photosphere is defined as  $\tau_l = \sigma_T n'_l r / (2\Gamma) = 1$ .

We have  $r_{\text{ph}} < r_s$  in the low baryon load case ( $\eta > \eta_*$ , where

$$\eta_* = \left( \frac{\sigma_T \mathcal{R} L \Gamma_a}{8\pi r_a m_p c^3} \right)^{1/4} \simeq 2.8 \times 10^3 L_{53}^{1/4} \left( \frac{r_{a,7}}{\Gamma_a} \right)^{-1/4} \mathcal{R}_1^{1/4}. \quad (2)$$

In this case, most of the luminosity is radiated at the photosphere. Leptons can frequently interact with photons even above the photosphere, and this Compton drag acceleration determines the remaining kinetic luminosity (Mészáros et al. 1993). The emission radius, luminosity, and peak energy of the photospheric emission and the final bulk Lorentz factor and remaining kinetic luminosity of the jet above the photosphere are given by (Mészáros & Rees 2000)

$$\begin{aligned} r_{\text{ph}} &= r_a \frac{\eta_*}{\Gamma_a} \left( \frac{\eta}{\eta_*} \right)^{-1/3}, & L_{\text{ph}} &\approx L, & \varepsilon_{\text{ph}} &\simeq 4 k T_a, \\ \Gamma_f &\simeq \eta_*, & L_k &\simeq L \left( \frac{\eta}{\eta_*} \right)^{-1}. \end{aligned} \quad (3)$$

On the other hand, in the high baryon load case  $\eta < \eta_*$ , we have  $r_{\text{ph}} > r_s$ . In this case most of the initial thermal energy has been converted to the kinetic energy below the photosphere. The corresponding quantities are given by<sup>3</sup>

$$\begin{aligned} r_{\text{ph}} &= r_a \frac{\eta_*}{\Gamma_a} \left( \frac{\eta}{\eta_*} \right)^{-3}, & L_{\text{ph}} &\simeq L \left( \frac{\eta}{\eta_*} \right)^{8/3}, \\ \varepsilon_{\text{ph}} &\simeq 4 k T_a \left( \frac{\eta}{\eta_*} \right)^{8/3}, & \Gamma_f &= \eta, & L_k &\approx L. \end{aligned} \quad (4)$$

For typical GRB jets with parameters  $L \sim 10^{51} - 10^{54} \text{ erg s}^{-1}$ , the photospheric emission can be bright with  $\varepsilon_{\text{ph}} \sim 100 \text{ keV} - 10 \text{ MeV}$  since the jets can have  $10^{-1} \lesssim r_{a,7}/\Gamma_a \lesssim 10^2$  and  $\eta \gtrsim \eta_*$  in principle.

<sup>2</sup> More accurately, one should use  $F_\varepsilon^{\text{th}} = 0.7(\varepsilon/kT_{\text{ph}})^3/[\exp(\varepsilon/kT_{\text{ph}}) - 1]$  where  $T_{\text{ph}} = \varepsilon_{\text{ph}}/3$  for the pure thermal component since  $\varepsilon = 4kT_{\text{ph}}$  is the peak energy of the  $\varepsilon F_\varepsilon$  spectrum instead of the  $F_\varepsilon$  spectrum. However, we obtain the same constraint  $\beta_{\text{ph}} \lesssim -2.5$  also from this calculation.

<sup>3</sup> We do not discuss the case  $r_{\text{ph}} > r_{sp} = 2W\eta^2$ , for which the radial spreading of shells (with the initial width  $W$ ) is significant, and the scaling law is different,  $r_{\text{ph}} \propto \eta^{-1/2}$  (Nakar et al. 2005).

### 3 TEMPORAL PROPERTIES

The GRB jet may be thought to consist of many successive shells with initial radial widths  $W \ll r_{\text{ph}}$ . This implies that the photospheric emission is temporally variable. After emerging from the photospheric regions, collisions between the ejected shells can produce internal shocks at  $r_i \gg r_{\text{ph}}$ . As we will show below, the leptons in the internal shock of two given shells can up-scatter their own photospheric emission, which was produced as they emerged from the photosphere. The UP emission can appear as a high-energy spectral component in the LAT energy range (see Section 4). The temporal properties of the emission in this model can be exemplified using a simple two-shell collision model (see Figure 1). For simplicity, we only consider the cases in which the two shells are both in the regime  $\eta < \eta_*$  or both in the regime  $\eta > \eta_*$ .

The duration of the observed photospheric emission from one shell is given by the light crossing time of the shell plus the angular spreading time,

$$\delta t_{\text{ph}} \sim \frac{W}{c} + \frac{r_{\text{ph}}}{2c\Gamma^2}. \quad (5)$$

This can be rewritten as  $\delta t_{\text{ph}} \sim (W/c) + r_{\text{ph}}/(2c\eta^2) \simeq (W/c) + (r_{\text{ph}}/r_i)t_v$  for  $\eta < \eta_*$ , and  $\delta t_{\text{ph}} \sim (W/c) + r_{\text{ph}}/(2c\Gamma_{\text{ph}}^2) \simeq (W/c) + (r_f/r_i)(\eta/\eta_*)^{1/3}t_v$  for  $\eta > \eta_*$ , where  $\Gamma_{\text{ph}} = \eta_*(\eta/\eta_*)^{-1/3}$ , and  $r_f = r_a\eta_*/\Gamma_a$  is the radius at which the Compton drag acceleration ceases.

Now we consider a two-shell collision. We assume that the two shells have similar initial radial width  $W$ , and the initial separation is  $ct_v$ . First consider the high baryon load case  $\eta < \eta_*$ . The rapid shell with Lorentz factor  $\Gamma_r = \eta_r$  catches up with the slower shell with Lorentz factor  $\Gamma_s = \eta_s$  (Hereafter subscripts ‘r’ and ‘s’ denote the quantities of the rapid and slow shells, respectively). Setting the zero time in the lab frame as the time when the rapid shell is at  $r = r_{\text{ph}}$ , the collision time is given by  $t_i = ct_v/[c(\beta_r - \beta_s)] \approx 2ct_v\eta_s^2$ , where we have used an approximation  $\eta \gg 1$ . The dissipation of the total kinetic energy is most efficient when the masses of the two shells are similar (c.f., Piran 2004). For typical cases, the ratio of the two Lorentz factors may be  $a_L = \eta_r/\eta_s \lesssim 5$ . Then the dissipation efficiency is given by  $\varepsilon_d \lesssim 0.25$ .

The photons which arrive at  $r = r_i$  at time  $t \geq t_i$  can be up-scattered by the energetic leptons in the internal shock. Let us define a length  $l_{\text{ns}}$ , measured from the front end of the rapid shell, as the radial scale of the region from which the photospheric photons do not interact with the leptons in the internal shock. Then we have  $r_{\text{ph}} - l_{\text{ns}} + ct_i = r_i = r_{\text{ph}} + c\beta_r t_i$ , which gives

$$l_{\text{ns}} = c(1 - \beta_r)t_i \approx a_L^{-2} ct_v. \quad (\eta < \eta_*) \quad (6)$$

We find that inverse Compton scattering is efficient for the case  $l_{\text{ns}} < W/2$  and inefficient for the case  $l_{\text{ns}} \gtrsim W/2$ .

A similar argument can be made also for the low baryon load case  $\eta > \eta_*$ . In this case the shells are accelerated similarly and cannot collide with each other below  $r_f = r_{\text{ph}}(\eta/\eta_*)^{1/3}$ . The internal shock radius is given by  $r_i \approx 2ct_v\eta_{*,s}^2$ , and we consider a case  $r_i \gg r_{f,r}$ . We have  $l_{\text{ns}} = ct_i - \int_0^{t_i} c\beta_r dt \approx (\eta_{*,s}^2/\eta_{*,r}^2)ct_v + (r_{\text{ph},r}\Gamma_{\text{ph},r}^{-2} - r_{f,r}\eta_{*,r}^{-2})$ . The second term represents a correction due to the velocity of the shell lower than  $\eta_{*,r}$  at  $r < r_{f,r}$ . The second term is

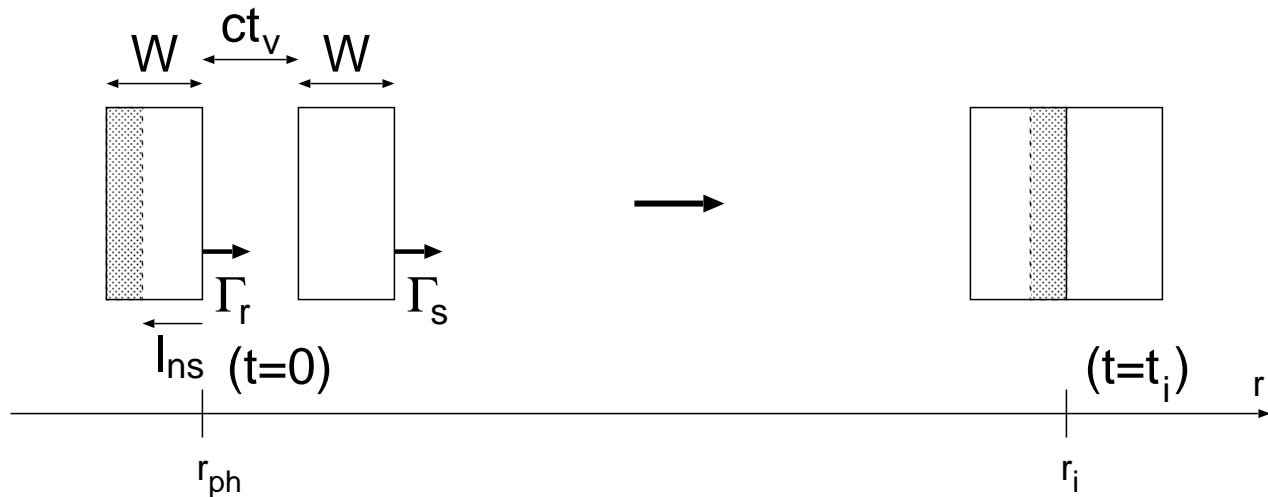


**Figure 1.** Interaction of the photospheric emission from two relativistically moving shells with the internal shock that the given shells themselves give rise to. The photons from the shaded region can be scattered by the leptons in the internal shock.

rewritten as  $r_{f,r}\eta_{*,r}^{-2}[(\eta_r/\eta_{*,r})^{1/3} - 1]$ , which cannot be dominant unless  $\eta \gg \eta_*$ , so that  $l_{ns}$  can typically be written as Equation (6) also in this case.

We have two parameter regimes for the scattering efficiency:

(i) *Efficient scattering regime*,  $l_{ns} < W/2$ . This includes the typical case  $W \sim ct_v$ . In this regime we may observe bright UP emission. The duration of the photospheric emission can be written as  $\delta t_{ph} \sim W/c$ , since we have assumed that  $r_i \gg r_{ph}$  for  $\eta < \eta_*$  and  $r_i \gg r_f$  for  $\eta > \eta_*$ . The onset of the UP emission is correlated with that of the photospheric emission pulse released from the rapid shell and delayed from that of the photospheric emission pulse released from the slow shell by  $t_{lag} = (W + ct_v + l_{ns})/c \sim (W/c) + t_v$ . The duration of the UP emission is given by the duration of the seed photons plus the angular spreading time

$$\delta t_{up} \sim \frac{W - l_{ns}}{c} + \frac{3r_i}{2c\Gamma_m^2} \simeq \frac{W}{c} + 3a_L^{-1}t_v. \quad (7)$$

The factor of  $\sim 3$  in the second term means that the UP emission has an anisotropic energy distribution in the comoving frame, being brightest at an angle  $\theta \sim 1/\Gamma_m$  from the line of sight in the observer frame (c.f., Brunetti 2000; Wang & Mészáros 2006; Fan et al. 2008; Toma et al. 2009b), where  $\Gamma_m \simeq (\Gamma_r\Gamma_s)^{1/2}$  is the Lorentz factor of the merged shell.

(ii) *Inefficient scattering regime*,  $l_{ns} \gtrsim W/2$ . In this regime, typically we may not observe bright UP emission. A caveat is that this regime includes a case  $l_{ns} \sim W + c\tilde{t}_v$ , in which we have a third shell behind the rapid shell of the two given shells apart by  $c\tilde{t}_v$ , and the photospheric emission from the third shell can be scattered by the leptons in the internal shock of the two given shells. This condition reduces to  $a_L^{-2}ct_v \sim W + c\tilde{t}_v$ , which is satisfied when  $\tilde{t}_v \ll t_v$ .

If the GRB jet is in the efficient scattering regime right from the start, when it first emerges, the delay timescale between the onsets of the first photospheric emission (in the MeV energy range) and the first UP emission (in the high-energy range) is  $\sim t_{lag} \sim (W/c) + t_v$ , which is comparable to  $\delta t_{ph}$  or  $t_v$ . However, *Fermi* observations show that

the LAT onset delays are much larger than the variability timescale apparent in the MeV energy light curves both for long and short GRBs. Therefore it is unlikely that the large delays of the high-energy emission onsets observed in many GRBs are due to the above simple kinematic effect of the jet whose physical parameters do not evolve. In our model, the large delays may be interpreted as the timescale on which the physical parameters of the jet temporally change, e.g.,  $W$  and  $t_v$  change from the inefficient scattering regime into the efficient scattering regime, or  $L$ ,  $r_a/\Gamma_a$ ,  $\eta$ , and  $\mathcal{R}$  change from the regime  $\eta > \eta_*$  into the regime  $\eta < \eta_*$  (see the following sections for details of the latter possibility). In these cases the UP emission can start, being still dim compared with the photospheric emission, at a time  $\sim t_{lag}$  after the first photospheric emission, and can become bright with the delay as observed.

## 4 SPECTRAL PROPERTIES

As shown above, the photospheric emission of the shells can be efficiently up-scattered by the leptons in the internal shocks of the same shells. Here we derive the generic broadband spectrum of the observed radiation arising in the internal shock including synchrotron and SSC emission for the efficient scattering regime.

### 4.1 Case of $\eta < \eta_*$

In this case the kinetic luminosity that can be dissipated into radiation by the internal shock is  $L_k \approx L$ . At  $r > r_{ph}$ , we have  $\sigma_T n'_l r / (2\eta) < 1$ , and the pair annihilation timescale is longer than the expansion timescale. Thus the pair population freezes out and we can write  $n'_l = \mathcal{R}L / (4\pi r^2 m_p c^3 \eta^2)$  even well above the photosphere. Hereafter we focus on the photospheric emission from the rapid shell, which is up-scattered by the leptons in the internal shock, so that  $\eta$  denotes  $\eta_r$  (The photospheric emission from the slower shell may be much dimmer). The internal

shock radius is estimated as  $r_i \simeq 2ct_v\eta_s^2 = 2ct_v\eta^2 a_L^{-2} \simeq 2 \times 10^{13} \eta_3^2 t_{v,-2} (a_L/5)^{-2}$  cm. Our assumption  $r_i \gg r_{\text{ph}}$  reduces to

$$\eta \gg 5 \times 10^2 L_{53}^{1/5} \mathcal{R}_1^{1/5} t_{v,-2}^{-1/5} \left(\frac{a_L}{5}\right)^{2/5}. \quad (8)$$

We assume that all the leptons participate in the non-thermal acceleration process in the internal shock and have the injected spectrum  $dn'_{i,i}/d\gamma = C\gamma^{-p}$  for  $\gamma \geq \gamma_m$ , where  $C$  is a constant. Then we have  $C\gamma_m^{1-p}/(p-1) = n'_i(r=r_i)$  and  $Cm_e c^2 \gamma_m^{2-p}/(p-2) = L\epsilon_d \epsilon_e / (4\pi r_i^2 c \eta^2)$ , where  $\epsilon_e$  is the fraction of the dissipation energy that is carried by leptons in the internal shock. (We consider a relatively weak internal shock, i.e.,  $a_L \lesssim 5$ , where we can neglect the change of the Lorentz factor of the jet for simplicity.) These lead to

$$\gamma_m = \frac{m_p}{m_e} \frac{p-2}{p-1} \mathcal{R}^{-1} \epsilon_d \epsilon_e \simeq 4 \mathcal{R}_1^{-1} \left(\frac{\epsilon_d \epsilon_e}{0.1}\right) f(p), \quad (9)$$

where  $f(p) = 13(p-2)/[3(p-1)]$ . If only a fraction of leptons are accelerated,  $\gamma_m$  is larger than this value.

We also assume that a fraction  $\epsilon_B$  of the dissipated energy is carried in the form of magnetic fields,  $U'_B = B'^2/(8\pi) = L\epsilon_d \epsilon_B / (4\pi r_i^2 c \eta^2)$ . The characteristic synchrotron energy of leptons with Lorentz factor  $\gamma$  is given by

$$\begin{aligned} \epsilon_{\text{syn}}(\gamma) &\simeq \frac{3heB'}{4\pi m_e c} \gamma^2 \eta \\ &\simeq 6 \times 10^{-1} \gamma^2 L_{53}^{1/2} \eta_3^{-2} t_{v,-2}^{-1} \left(\frac{a_L}{5}\right)^2 \left(\frac{\epsilon_d \epsilon_B}{0.1}\right)^{1/2} \text{ eV} \end{aligned} \quad (10)$$

The leptons emit the UP emission, synchrotron emission, and SSC emission. The comoving energy density of the synchrotron emission can be written by

$$U'_{\text{syn}} = t'_{\text{dyn}} \frac{4}{3} \sigma_T c U'_B \int \gamma^2 \frac{dn'_i}{d\gamma} d\gamma = x U'_B, \quad (11)$$

where  $t'_{\text{dyn}} \simeq r_i/(2c\eta)$  is the dynamical timescale of the internal shock and  $dn'_i/d\gamma$  is the lepton energy distribution averaged over the dynamical timescale. The quantity  $x$  is calculated as

$$x = \frac{4}{3} \sigma_T \frac{r_i}{2\eta} \int \gamma^2 \frac{dn'_i}{d\gamma} d\gamma \simeq \frac{4(p-1)}{3(p-2)} \tau_{i,i} \gamma_m \gamma_c h(\gamma_m, \gamma_c), \quad (12)$$

where  $\gamma_c$  is the cooling Lorentz factor of the leptons and  $\tau_{i,i}$  is the Thomson optical depth at  $r_i$  (which can be written as  $\tau_{i,i} = r_{\text{ph}}/r_i$  in the case of  $\eta < \eta_*$ ). We have assumed  $p > 2$  and defined the function  $h(\gamma_m, \gamma_c)$  as  $h = 1$  for  $\gamma_c \ll \gamma_m$ ,  $h = p/(p-1)$  for  $\gamma_c \approx \gamma_m$ ,  $h = (\gamma_c/\gamma_m)^{2-p}/(3-p)$  for  $\gamma_m \ll \gamma_c$  and  $p < 3$ , and  $h = (p-2)\gamma_m/[(p-3)\gamma_c]$  for  $\gamma_m \ll \gamma_c$  and  $p \geq 3$ . Similarly we have the SSC emission energy density  $U'_{\text{SSC}} = x U'_{\text{syn}}$ , where we have assumed that the Klein-Nishina (KN) effect is not significant. This is valid for the parameters adopted in the case study of observed LAT GRBs in Section 5. We also have the UP emission energy density  $U'_{\text{up}} = x U'_{\text{ph}}$ , where we have assumed that the KN effect is not significant also for the UP emission. This is found to be valid for observed LAT GRBs in Section 5. We also have neglected the anisotropy of the UP photon energy distribution, for simplicity. This anisotropy leads to the reduction of the observed UP luminosity averaged over a pulse than the isotropic assumption by a factor of  $\sim 2$  (Fan et al. 2008; Toma et al. 2009b), which we will neglect

below. By using the relation, e.g.,  $L_{\text{ph}} = 4\pi r_i^2 c \eta^2 U'_{\text{ph}}$ , we have

$$\begin{aligned} L_{\text{up}} &\simeq x L_{\text{ph}}, \\ L_{\text{syn}} &\simeq \epsilon_d \epsilon_B x L \simeq k x L_{\text{ph}}, \\ L_{\text{SSC}} &\simeq \epsilon_d \epsilon_B x^2 L \simeq k x^2 L_{\text{ph}}, \end{aligned} \quad (13)$$

where we have defined

$$k \equiv \frac{\epsilon_d \epsilon_B}{(\eta/\eta_*)^{8/3}}. \quad (14)$$

The photospheric luminosity is given by  $L_{\text{ph}} \simeq L(\eta/\eta_*)^{8/3}$  (see Eq. 4).

We require to estimate the cooling Lorentz factor  $\gamma_c$  for specifying the lepton energy distribution averaged over the dynamical timescale and the various emission luminosities. Since the cooling rate for one lepton with Lorentz factor  $\gamma$  is  $P(\gamma) = (4/3)\sigma_T c \gamma^2 (U'_B + U'_{\text{syn}} + U'_{\text{ph}})$ , the cooling Lorentz factor can be estimated by  $\gamma_c m_e c^2 = P(\gamma_c) r_i / (2c\eta)$ . This reduces to

$$\gamma_c \simeq \frac{3m_e \mathcal{R}}{4m_p \tau_{i,i} (\eta/\eta_*)^{8/3}} \frac{1}{k(1+x) + 1}. \quad (15)$$

If  $k \gg 1$ , we can take  $k(1+x) + 1 \approx k(1+x)$ . Then Eq. (12) reduces to  $x = (\epsilon_e h / \epsilon_B) / (1+x)$ , and we have

$$x \approx \begin{cases} \sqrt{\epsilon_e h / \epsilon_B}, & (x \gg 1), \\ \epsilon_e h / \epsilon_B, & (x \ll 1). \end{cases} \quad (k \gg 1) \quad (16)$$

This is a general result for the case in which the radiation is dominated by synchrotron and SSC emissions, as developed by Sari & Esin (2001). In the first case,  $x \gg 1$ , we have  $kx^2 \gg kx \gg x \gg 1$ , so that the order of the four emission luminosities is found to be  $L_{\text{SSC}} \gg L_{\text{syn}} \gg L_{\text{up}} \gg L_{\text{ph}}$ . The condition  $k \gg 1$  and  $x \gg 1$  is equivalent to  $\epsilon_d \epsilon_e h \gg \epsilon_d \epsilon_B \gg (\eta/\eta_*)^{8/3}$ . The second case,  $x \ll 1$ , should be divided into three sub-cases; ( $kx \gg 1$  and  $kx^2 \gg 1$ ), ( $kx \gg 1$  and  $kx^2 \ll 1$ ), and ( $kx \ll 1$ ). The orders of the luminosities in these cases are summarized in Table 1, which are labeled as cases 5, 6, 7, and 8, respectively. In the Table we define  $\mathcal{G} \equiv (\eta/\eta_*)^{8/3}$ ,  $\mathcal{E} \equiv \epsilon_d \epsilon_e h$ , and  $\mathcal{B} \equiv \epsilon_d \epsilon_B$  for clarification.

If  $k \ll 1$ , we can take  $k(1+x) + 1 \approx kx + 1$  in Eq. (15). This case should be divided into further two cases,  $kx \gg 1$  or  $kx \ll 1$ . We can take  $k(1+x) + 1 \approx kx$  in the former case and  $k(1+x) + 1 \approx 1$  in the latter case. In the former case, we have

$$x \approx \sqrt{\epsilon_e h / \epsilon_B} \quad (k \ll 1, kx \gg 1). \quad (17)$$

This is shown as case 4 in Table 1. In the latter case, we have

$$x \approx \frac{\epsilon_d \epsilon_e h}{(\eta/\eta_*)^{8/3}} \quad (k \ll 1, kx \ll 1). \quad (18)$$

This case should be divided into three sub-cases; ( $x \ll 1$ ), ( $x \gg 1$  and  $kx^2 \ll 1$ ), and ( $x \gg 1$  and  $kx^2 \gg 1$ ). These are labeled as cases 1, 2, and 3, respectively in Table 1. We can calculate the cooling Lorentz factor  $\gamma_c$  for each case by Eq. (15).

The ordering of the emission luminosities for various cases listed in Table 1 divides the GRB emission models into two groups. Since the synchrotron and SSC emission components can have very broad spectra, so that a condition  $L_{\text{ph}} \gg \max(L_{\text{syn}}, L_{\text{SSC}})$  is necessary for the photospheric emission to be dominant in the MeV energy range

**Table 1.** Ordering of emission luminosities for various cases of  $\mathcal{G} = (\eta/\eta_*)^{8/3}$ ,  $\mathcal{E} = \epsilon_d \epsilon_e h$ , and  $\mathcal{B} = \epsilon_d \epsilon_B$ .

Case	$\mathcal{G}$	$k(\text{or } k'), x$	Luminosities	$\mathcal{E}$ and $\mathcal{B}$	
1	$\eta < \eta_*(\mathcal{G} < 1)$	$k \ll 1, kx \ll 1$	$x \ll 1$	$L_{\text{ph}} \gg L_{\text{up}} \gg L_{\text{syn}} \gg L_{\text{ssc}}$	$\mathcal{G} \gg \max(\mathcal{E}, \mathcal{B})$
2			$x \gg 1, kx^2 \ll 1$	$L_{\text{up}} \gg L_{\text{ph}} \gg L_{\text{ssc}} \gg L_{\text{syn}}$	$\mathcal{E} \gg \mathcal{G} \gg (\mathcal{E}^2 \mathcal{B})^{1/3} \gg \mathcal{B}$
3			$x \gg 1, kx^2 \gg 1$	$L_{\text{up}} \gg L_{\text{ssc}} \gg L_{\text{ph}} \gg L_{\text{syn}}$	$\mathcal{E} \gg (\mathcal{E}^2 \mathcal{B})^{1/3} \gg \mathcal{G} \gg \mathcal{B}$
4		$k \ll 1, kx \gg 1$		$L_{\text{ssc}} \gg L_{\text{up}} \gg L_{\text{syn}} \gg L_{\text{ph}}$	$\mathcal{E} \gg (\mathcal{E} \mathcal{B})^{1/2} \gg \mathcal{G} \gg \mathcal{B}$
5		$k \gg 1$	$x \gg 1$	$L_{\text{ssc}} \gg L_{\text{syn}} \gg L_{\text{up}} \gg L_{\text{ph}}$	$\mathcal{E} \gg \mathcal{B} \gg \mathcal{G}$
6			$x \ll 1, kx \gg 1, kx^2 \gg 1$	$L_{\text{syn}} \gg L_{\text{ssc}} \gg L_{\text{ph}} \gg L_{\text{up}}$	$\mathcal{B} \gg \mathcal{E} \gg \mathcal{E}^2/\mathcal{B} \gg \mathcal{G}$
7			$x \ll 1, kx \gg 1, kx^2 \ll 1$	$L_{\text{syn}} \gg L_{\text{ph}} \gg L_{\text{ssc}} \gg L_{\text{up}}$	$\mathcal{B} \gg \mathcal{E} \gg \mathcal{G} \gg \mathcal{E}^2/\mathcal{B}$
8			$x \ll 1, kx \ll 1$	$L_{\text{ph}} \gg L_{\text{syn}} \gg L_{\text{up}} \gg L_{\text{ssc}}$	$\mathcal{B} \gg \mathcal{G} \gg \mathcal{E}$
9	$\eta > \eta_*(\mathcal{G} > 1)$	$k' \ll 1, k'x \ll 1$	$x \ll 1$	$L_{\text{ph}} \gg L_{\text{up}} \gg L_{\text{syn}} \gg L_{\text{ssc}}$	$\mathcal{G} \gg \max(\mathcal{E}, \mathcal{B})$

rather than the synchrotron or SSC emission components. Thus cases 1, 2, and 8 are included in the photospheric emission models, while cases 3, 4, 5, 6, and 7 are included in the synchrotron-SSC emission models. In this paper we focus on the former cases, and in particular cases 1 and 2, for which the UP emission component is dominant in the high-energy range. We will see that cases 1 and 2 can be consistent with the spectra of some LAT GRBs in Section 5. Here we show the description of the cooling Lorentz factor in cases 1 and 2,

$$\begin{aligned} \gamma_c &\simeq \frac{3m_e \mathcal{R}}{4m_p \tau_{l,i} (\eta/\eta_*)^{8/3}} \\ &\simeq 3 L_{53}^{-1/3} \left( \frac{r_{a,7}}{\Gamma_a} \right)^{-2/3} \eta_3^{7/3} \mathcal{R}_1^{2/3} t_{v,-2} \left( \frac{a_L}{5} \right)^{-2}. \end{aligned} \quad (19)$$

The UP luminosity is simply written as

$$L_{\text{up}} \simeq L \epsilon_d \epsilon_e h. \quad (20)$$

Figure 2 shows an example of a broadband spectrum of the emission from the GRB jet for case 1. The parameters are taken as  $L_{53} = 3$ ,  $\eta_3 = 3$ ,  $r_{a,7}/\Gamma_a = 1$ ,  $\mathcal{R}_1 = 2$ ,  $\beta_{\text{ph}} = -2.5$ ,  $t_{v,-2} = 1$ ,  $p = 2.3$ ,  $\epsilon_d \epsilon_e = 0.1$ ,  $\epsilon_d \epsilon_B = 0.03$ , and  $a_L = 5$ . The source redshift is set to be  $z = 2$ . For these parameters, we have  $(\eta/\eta_*)^{8/3} \simeq 0.4 > \max(\epsilon_d \epsilon_e h, \epsilon_d \epsilon_B)$ , and  $r_{\text{ph}} \simeq 1 \times 10^{11}$  cm and  $r_i \simeq 2 \times 10^{14}$  cm, which satisfy our assumption  $r_i \gg r_{\text{ph}}$  (Eq. 8). We generate the spectra of the four emission components using the approximate forms of the individual components. The photospheric emission is approximated as a smoothed broken power-law spectrum

$$\epsilon F_\epsilon^{\text{ph}} = A_{\text{ph}} \left( \frac{\epsilon}{\epsilon_{\text{ph}}} \right)^3 \left[ 1 + \left( \frac{\epsilon}{\epsilon_{\text{ph}}} \right)^s \right]^{\frac{\beta_{\text{ph}} - 1}{s}}, \quad (21)$$

where a constant  $A_{\text{ph}}$  is given for the peak of  $\epsilon F_\epsilon^{\text{ph}}$  to be equal to  $L_{\text{ph}}/(4\pi d_L^2)$  ( $d_L$  is the luminosity distance) and we set  $s = 2$ . The UP, synchrotron, and SSC components are approximated similarly as smoothed broken power-law spectra with the  $\epsilon F_\epsilon$  peak values being equal to  $L_{\text{up}}/(4\pi d_L^2)$ ,  $L_{\text{syn}}/(4\pi d_L^2)$ , and  $L_{\text{ssc}}/(4\pi d_L^2)$ , respectively. The  $\epsilon F_\epsilon$  spectral indices of the UP emission are given by 2 for  $\epsilon < \epsilon_{\text{up},l}$ ,  $(3 - q)/2$  for  $\epsilon_{\text{up},l} < \epsilon < \epsilon_{\text{up},h}$ ,  $(2 - p)/2$  for  $\epsilon_{\text{up},h} < \epsilon < \epsilon_{\text{up,KN}}$ , and  $-p - 1$  for  $\epsilon > \epsilon_{\text{up,KN}}$ , where  $\epsilon_{\text{up},l} \simeq \epsilon_{\text{ph}} \gamma_l^2$ ,  $\epsilon_{\text{up},h} \simeq \epsilon_{\text{ph}} \gamma_h^2$  ( $\gamma_l \equiv \min(\gamma_m, \gamma_c)$  and  $\gamma_h \equiv \max(\gamma_m, \gamma_c)$ ),  $\epsilon_{\text{up,KN}} \simeq (\eta m_e c^2)^2 / \epsilon_{\text{ph}}$ , and  $q = p$  ( $q = 2$ ) for the slow cooling case  $\gamma_m < \gamma_c$  (for the fast cooling case  $\gamma_c < \gamma_m$ ). This is valid for the case of  $\beta_{\text{ph}} \leq -(2 + p)/2$ , which is satisfied for our case  $\beta \lesssim -2.5$  and  $2 < p < 3$ . The spec-

tral indices of the synchrotron and SSC emission are found in Sari & Esin (2001). Figure 2 shows that the overall spectrum consists of a photospheric component in the mid-range, and synchrotron and UP components in the low and high energy ranges, respectively. We will use this approximate method to have a rough overall spectrum and to show that the emission from the photosphere and internal shock can be consistent with the time-resolved spectra of observed LAT GRBs, GRB 080916C, GRB 090510, and GRB 090902B in section 5.

The high-energy photospheric photons are absorbed by the  $e^\pm$  pair creation at the photosphere. Assuming that the photons are isotropic in the comoving frame of the jet, the opacity for the photons with the comoving frame energy  $\epsilon'$  can be estimated by  $\tau_{\gamma\gamma}^{\text{ph}}(\epsilon') \simeq 0.1 \sigma_T \epsilon'_{\text{ann}} n'_{\text{ph}}(r_{\text{ph}}; \epsilon'_{\text{ann}}) r_{\text{ph}} / (2\eta)$ , where  $\epsilon'_{\text{ann}} = m_e^2 c^4 / \epsilon'$ , and  $n'_{\text{ph}}(r_{\text{ph}}; \epsilon') \simeq L_{\text{ph}}(\epsilon' / \epsilon'_{\text{ph}})^{\beta_{\text{ph}}} / (4\pi r_{\text{ph}}^2 c \eta^2 \epsilon'^2_{\text{ph}})$  is the comoving photon density per unit energy around  $\epsilon'$  at the photosphere (cf., Lithwick & Sari 2001). Here we only consider the high-energy part of the photospheric emission (with the index  $\beta_{\text{ph}}$ ) as target photons, since the photon density  $\sim \epsilon' n'_{\text{ph}}(r_{\text{ph}}; \epsilon')$  peaks at  $\epsilon'_{\text{ph}}$ . If a calculated main target photon (comoving) energy for the pair creation break energy is smaller than  $\epsilon'_{\text{ph}}$ , the region is optically thin for the pair creation. The pair creation break energy, defined by  $\tau_{\gamma\gamma}^{\text{ph}}(\epsilon') = 1$ , is given by

$$\begin{aligned} \epsilon_{\gamma\gamma}^{\text{ph}} &\simeq \left[ 0.1 \frac{m_p}{m_e} \left( \frac{\eta}{\eta_*} \right)^{8/3} \mathcal{R}^{-1} \eta^{2\beta_{\text{ph}}+3} \right. \\ &\quad \left. \left( \frac{\epsilon_{\text{ph}}}{m_e c^2} \right)^{-2-\beta_{\text{ph}}} \right]^{\frac{1}{1+\beta_{\text{ph}}}} \times m_e c^2 \\ &\simeq 3 \left[ (9 \times 10^3)^{\frac{3+\beta_{\text{ph}}}{2}} \left( \frac{\eta}{\eta_*} \right)^{8/3} \mathcal{R}_1^{-1} \eta_3^{2\beta_{\text{ph}}+3} \right. \\ &\quad \left. \left( \frac{\epsilon_{\text{ph}}}{1 \text{ MeV}} \right)^{-2-\beta_{\text{ph}}} \right]^{\frac{1}{1+\beta_{\text{ph}}}} \text{ GeV}. \end{aligned} \quad (22)$$

For the spectral model of the photospheric emission, we assume a spectral cutoff at this energy.

The  $e^\pm$  pair creation opacity for the high-energy UP photons at the internal shock region can be estimated similarly. The main target photons for the high-energy UP photons may be either the photospheric emission incident into the internal shock region or the UP emission itself. Since the incident photospheric emission is highly anisotropic at the

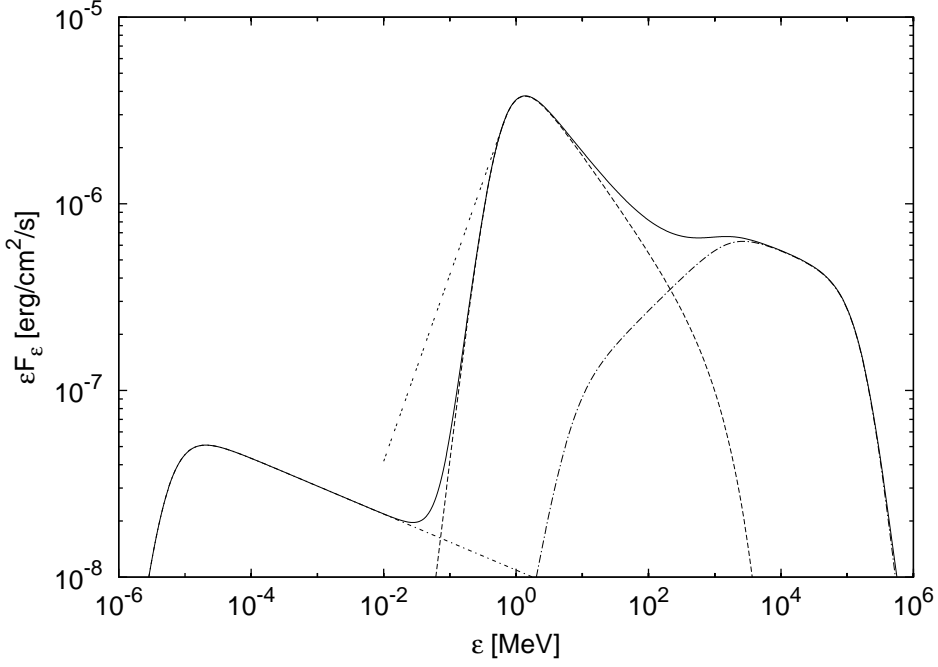


**Figure 2.** Example of the model spectrum of case 1 (see Table 1). The spectrum consists of the photospheric emission (dashed line), the UP emission (dot-long-dashed line), and the synchrotron emission (dot-short-dashed line). The SSC emission is not shown since it is too dim. The parameters are  $L_{53} = 3$ ,  $\eta_3 = 3$ ,  $r_{a,\gamma}/\Gamma_a = 1$ ,  $\mathcal{R}_1 = 2$ ,  $\beta_{\text{ph}} = -2.5$ ,  $t_{v,-2} = 1$ ,  $p = 2.3$ ,  $\epsilon_d \epsilon_e = 0.1$ ,  $\epsilon_d \epsilon_B = 0.03$ ,  $a_L = 5$ , and  $z = 2$ . The characteristic quantities are  $\eta_* \simeq 4.3 \times 10^3$ ,  $L_{\text{ph}} \simeq L(\eta/\eta_*)^{8/3} \simeq 1 \times 10^{53}$  erg s $^{-1}$ ,  $\epsilon_{\text{ph}} \simeq 4kT_a(\eta/\eta_*)^{8/3} \simeq 4$  MeV,  $\epsilon_{\gamma\gamma}^{\text{ph}} \simeq 5$  GeV,  $L_{\text{up}} \simeq L\epsilon_d \epsilon_e h \simeq 2 \times 10^{52}$  erg s $^{-1}$ ,  $\epsilon_{\text{up},m} \simeq \epsilon_{\text{ph}} \gamma_m^2 \simeq 20$  MeV,  $\epsilon_{\text{up},c} \simeq \epsilon_{\text{ph}} \gamma_c^2 \simeq 5$  GeV,  $\epsilon_{\text{up},\text{KN}} \simeq (\eta m_e c^2)^2 / \epsilon_{\text{ph}} \simeq 600$  GeV,  $L_{\text{syn}} \simeq \epsilon_d \epsilon_B L_{\text{up}} / (\eta/\eta_*)^{8/3} \simeq 1 \times 10^{51}$  erg s $^{-1}$ ,  $\epsilon_{\text{syn},c} \simeq \epsilon_{\text{syn}}(\gamma_c) \simeq 80$  eV, and  $\epsilon_{\text{syn},a} \simeq 60$  eV. The intra-source  $e^\pm$  pair creation opacity is estimated to be less than unity. We do not take into account the absorption by the  $e^\pm$  pair creation through propagating in the intergalactic medium. The two-dot line describes a low-energy spectrum with an index  $\alpha_{\text{ph}} = -1.0$ , typical of observed GRBs, whose possible origins are discussed in section 6.

internal shock region and the collision angle of the two photons is typically very small, so that the pair creation opacity will be significantly reduced from that with the isotropic assumption (Zou et al. 2011) (see also Granot et al. 2008; Ackermann et al. 2011). Yet, for simplicity, we estimate the pair creation opacity by the interaction with the photospheric emission with the isotropic assumption, which provides a possible largest opacity. On the other hand, the target UP photons are much less anisotropic. We derive a minimum possible value of the break energy, which can be obtained as the lower one of the break energies caused by pair creations with the photospheric and the UP photons calculated under the isotropic assumption. The photon densities per unit energy in the relevant energy range are given by  $n'_{\text{ph}}(r_i; \epsilon') \simeq L_{\text{ph}}(\epsilon'/\epsilon'_{\text{ph}})^{\beta_{\text{ph}}} / (4\pi r_i^2 c \eta^2 \epsilon'^2_{\text{ph}})$  and  $n'_{\text{up}}(r_i; \epsilon') \simeq L_{\text{up}}(\epsilon'/\epsilon'_{\text{up}})^{-(1+q)/2} / (4\pi r_i^2 c \eta^2 \epsilon'^2_{\text{up},h})$  for the photospheric and UP emission, respectively. Thus the possible minimum break energy is estimated by  $\epsilon_{\gamma\gamma}^{\text{min}} \simeq \min(\epsilon_{\gamma\gamma,\text{ph}}^{\text{min}}, \epsilon_{\gamma\gamma,\text{up}}^{\text{min}})$  and

$$\begin{aligned} \epsilon_{\gamma\gamma,\text{ph}}^{\text{min}} &\simeq \left[ \frac{3}{40} \gamma_c^{-1} \eta^{2\beta_{\text{ph}}+3} \left( \frac{\epsilon_{\text{ph}}}{m_e c^2} \right)^{-2-\beta_{\text{ph}}} \right]^{\frac{1}{1+\beta_{\text{ph}}}} \times m_e c^2 \\ &\simeq 1 \times 10^2 \left[ 4^{\frac{3+\beta_{\text{ph}}}{2}} \left( \frac{\gamma_c}{10} \right)^{-1} \eta_3^{2\beta_{\text{ph}}+3} \right. \\ &\quad \left. \left( \frac{\epsilon_{\text{ph}}}{1 \text{ MeV}} \right)^{-2-\beta_{\text{ph}}} \right]^{\frac{1}{1+\beta_{\text{ph}}}} \text{ GeV}, \end{aligned}$$

$$\begin{aligned} \epsilon_{\gamma\gamma,\text{up}}^{\text{min}} &\simeq \left[ \frac{3}{40} \gamma_c^{-1} x \eta^{2-q} \left( \frac{\epsilon_{\text{up},h}}{m_e c^2} \right)^{\frac{q-3}{2}} \right]^{\frac{2}{1-q}} \times m_e c^2 \\ &\simeq 2 \times 10^1 \left[ (4 \times 10^{-3})^{2-q} \left( \frac{\gamma_c}{10} \right)^{-1} x \eta_3^{2-q} \right. \\ &\quad \left. \left( \frac{\epsilon_{\text{up},h}}{1 \text{ GeV}} \right)^{\frac{q-3}{2}} \right]^{\frac{2}{1-q}} \text{ TeV}, \end{aligned} \quad (23)$$

where  $x$  is given by Eq. (18). The opacity of the interaction with the photospheric emission (the UP emission) for all the high-energy photons is less than unity if  $\epsilon_{\gamma\gamma,\text{ph}}^{\text{min}} > (\eta^2 m_e c^2)^2 / \epsilon_{\text{ph}}$  ( $\epsilon_{\gamma\gamma,\text{up}}^{\text{min}} > (\eta^2 m_e c^2)^2 / \epsilon_{\text{up},l}$ ).

The energy  $\epsilon_{\text{syn},a}$  below which the synchrotron self-absorption effect is significant can be estimated by equating synchrotron flux to the blackbody flux of the characteristic electrons in the shocked region,  $F_{\epsilon_{\text{syn},a}} = [(1+z)^3/d_L^2] 2\pi m_e \gamma_{ch} (\epsilon_{\text{syn},a}/h)^2 (r_i^2/\eta)$  (e.g., Mészáros & Rees 1997). The characteristic Lorentz factor  $\gamma_{ch}$  of leptons is given by  $\gamma_a$  whose synchrotron energy is  $\epsilon_{\text{syn},a}$  in the case of  $\gamma_a > \gamma_l$  and otherwise by  $\gamma_l$ . We show a formula of the ratio of  $\epsilon_{\text{syn},a}$  to  $\epsilon_{\text{syn},h} = \epsilon_{\text{syn}}(\gamma_h)$ , by which we can calculate  $\epsilon_{\text{syn},a}$  in a typical case  $\gamma_a > \gamma_l$ ,

$$\frac{\epsilon_{\text{syn},a}}{\epsilon_{\text{syn},h}} \simeq \left[ \frac{8\pi\sqrt{3}}{9} \frac{e\tau_{l,i}}{\sigma_T B'} \gamma_l^{q-1} \gamma_h^{-q-4} \right]^w, \quad (24)$$

where  $w = 2/(q+4)$  for  $\gamma_l < \gamma_a < \gamma_h$  and  $w = 2/(p+5)$  for  $\gamma_a > \gamma_h$ . The value of  $\epsilon_{\text{syn},a}$  is important for estimating the

observed synchrotron flux at the optical frequency (see the above example shown in Figure 2).

#### 4.2 Case of $\eta > \eta_*$

In this case the kinetic luminosity that can be dissipated in the internal shock is  $L_k \approx L(\eta/\eta_*)^{-1}$ . The internal shock radius is estimated to be  $r_i \simeq 2ct_v\eta_*^2 a_L^{-2}$ , and our assumption  $r_i \gg r_f$  reduces to

$$\frac{r_a}{\Gamma_a} \ll 2ct_v\eta_* a_L^{-2} \simeq 6 \times 10^{11} t_{v,-2}\eta_{*,3} a_L^{-2} \text{ cm.} \quad (25)$$

The minimum injection Lorentz factor of the leptons is given by Eq.(9). The magnetic field energy density is  $U'_B = L\epsilon_d\epsilon_B/(4\pi r_i^2 c\eta\eta_*)$ , and then the characteristic synchrotron energy of leptons with Lorentz factor  $\gamma$  is given by

$$\begin{aligned} \epsilon_{\text{syn}}(\gamma) &\simeq \frac{3heB'}{4\pi m_e c} \gamma^2 \eta_* \\ &\simeq 5 \times 10^{-1} \gamma^2 L_{53}^{1/8} \left(\frac{r_{a,7}}{\Gamma_a}\right)^{3/8} \eta_3^{-1/2} \mathcal{R}_1^{-3/8} \\ &\quad \times t_{v,-2}^{-1} a_L^2 \left(\frac{\epsilon_d\epsilon_B}{0.1}\right)^{1/2} \text{ eV.} \end{aligned} \quad (26)$$

The photospheric, UP, synchrotron, and SSC luminosities are estimated to be  $L_{\text{ph}} \approx L$ ,  $L_{\text{up}} \simeq xL$ ,  $L_{\text{syn}} \simeq k'xL$ , and  $L_{\text{ssc}} \simeq k'x^2L$ , where  $x$  is calculated by Eq.(12), and we have defined

$$k' \equiv \frac{\epsilon_d\epsilon_B}{\eta/\eta_*}. \quad (27)$$

The cooling Lorentz factor of leptons is

$$\gamma_c \simeq \frac{3m_e \mathcal{R}}{4m_p \tau_{l,i}(\eta/\eta_*)} \frac{1}{k'(1+x) + 1}, \quad (28)$$

where the optical depth at  $r_i$  can be written as  $\tau_{l,i} = (r_{\text{ph}}/r_i)(\eta/\eta_*)^{-2/3}$ . The equations for the luminosities and  $\gamma_c$  are the same as those for the case  $\eta < \eta_*$  by replacing  $(\eta/\eta_*)^{8/3}$  by  $\eta/\eta_*$  and  $k$  by  $k'$ , so that the same argument for dividing cases for the order of the four luminosities can be made. In this case, however,  $\eta > \eta_*$  leads to  $k' < 1$  and  $\epsilon_d\epsilon_e h/(\eta/\eta_*) < 1$ . Then we only have the case of  $k' \ll 1$  and  $k'x \ll 1$ , which we include as case 9 in Table 1. In this case the MeV and high-energy emissions may be dominated by the photospheric and UP components, respectively, similar to case 1. (The case of  $k' \ll 1$  and  $k'x \gg 1$  leads to  $x \approx \sqrt{\epsilon_e h/\epsilon_B} (\gg 1)$ , which is not consistent with the condition  $k'x^2 = \epsilon_d\epsilon_e h/(\eta/\eta_*) < 1$ .) The cooling Lorentz factor is calculated by

$$\gamma_c \simeq \frac{3m_e \mathcal{R}}{4m_p \tau_{l,i}(\eta/\eta_*)} \simeq 7 \times 10^2 L_{53}^{1/4} \left(\frac{r_{a,7}}{\Gamma_a}\right)^{-5/4} \mathcal{R}_1^{5/4} t_{v,-2} a_L^{-2}. \quad (29)$$

The parameter  $x$  and the UP luminosity are given by

$$x \approx \frac{\epsilon_d\epsilon_e h}{\eta/\eta_*}, \quad (30)$$

$$L_{\text{up}} \simeq L \left(\frac{\eta}{\eta_*}\right)^{-1} \epsilon_d\epsilon_e h. \quad (31)$$

The pair creation break energies of the photospheric and the UP emission can be estimated by Eq. (22) with replacing  $(\eta/\eta_*)^{8/3}$  by  $(\eta/\eta_*)^{-(8/3)(1+\beta_{\text{ph}})}$  and Eq. (23) with replacing  $\eta$  by  $\eta_*$  and setting  $x$  to be Eq. (30), respectively. The synchrotron self-absorption energy can be estimated by the same equation as Eq. (24).

## 5 CASE STUDIES

The previous sections have provided a general formulation of the emission from the photosphere and internal shock of the GRB jet. Here we focus on the cases in which the emission in the MeV energy range and in the high-energy range are dominated by the photospheric and the UP emission components, respectively, instead of the synchrotron or SSC emission components (i.e., cases 1, 2, and 9 in Table 1). We then show that such cases can be consistent with the observed time-resolved spectra of three of the best observed *Fermi*/LAT GRBs, especially in the energy range at and above the MeV spectral peaks. The detailed analysis results of the observed spectra of brightest LAT GRBs, GRB 080916C, GRB 090902B and GRB 090510 have been published (Abdo et al. 2009b,c; Ackermann et al. 2010a), and it is to these data that we apply our formulation. We assume that essentially the parameters  $W$  and  $ct_v$  are in the efficient scattering regime (see section 3), unless otherwise stated.

### 5.1 GRB 080916C

This burst is a long GRB that occurred at a redshift  $z \simeq 4.35$  (corresponding to  $d_L \simeq 1.2 \times 10^{29}$  cm). The spectral analysis shows that all the spectra of the five time-bins can be fitted by Band functions (Abdo et al. 2009b). These time-binned spectra are shown by the thin lines in Figure 3. The high-energy spectral index of the second time-bin 3.6 – 7.7 s,  $\beta \simeq -2.2$ , is significantly larger than that of the first time-bin 0.0 – 3.6 s,  $\beta \simeq -2.6$ . This spectral hardening corresponds to the observed delay of the onset of the LAT emission with respect to that of the GBM emission. The delay timescale in the cosmological rest frame is  $\sim 5/(1+z)$  s  $\sim 1$  s. The high-energy spectral index seems stable after the second time-bin. We will see that the first time-bin spectrum is consistent with having only a photospheric component, while the subsequent time-bin spectra can be modeled as a photospheric plus a UP component, which mimic a smooth Band function.

We first find the parameter values appropriate for the *second* time-bin spectrum. In our adiabatic jet model, we have a constraint  $\beta_{\text{ph}} \lesssim -2.5$  (see Section 2). Thus the observed hard high-energy spectrum of this time-bin with  $\beta \simeq -2.2$  has to be made by a combination of the photospheric and UP emission. The spectrum can be fitted in this way as shown by the thick dashed line in Figure 3. The following conditions are required for producing such a spectrum:  $L_{\text{ph}} \sim 4.5 \times 10^{53}$  erg s $^{-1}$ ,  $\epsilon_{\text{ph}} \sim 6.3$  MeV,  $\beta_{\text{ph}} \simeq -2.5$ ,  $L_{\text{up}} \sim 1.1 \times 10^{53}$  erg s $^{-1}$ ,  $\epsilon_{\text{up},c} \sim 2.5$  GeV,  $\epsilon_{\text{up},m} \lesssim 42$  MeV (which correspond to  $\gamma_c \sim 20$  and  $\gamma_m \lesssim 2.6$ ), and  $p \simeq 2.8$ . Significant deviations from these conditions lead to a bumpy spectrum and/or deviate from the observed data with errors taken into account (see below for other conditions). The conditions indicate the slow-cooling case of the electron distribution, i.e.,  $\gamma_m < \gamma_c$ . The fast-cooling case is not favored since it has a harder spectrum at  $\epsilon_{\text{up},c} < \epsilon < \epsilon_{\text{up},m}$  which makes a dip in the spectrum. The ratio of the two luminosities is  $L_{\text{up}}/L_{\text{ph}} = x \sim 0.2$ , which indicates  $\eta < \eta_*$  for a reasonable value of  $\epsilon_d\epsilon_e \lesssim 0.1$  for the internal shock (see Equations 18 and 30). Thus this spectrum corresponds to case 1 (see Table 1). Equations for case 1, (4), (20), (9), and (19), translate the above conditions into five constraints on

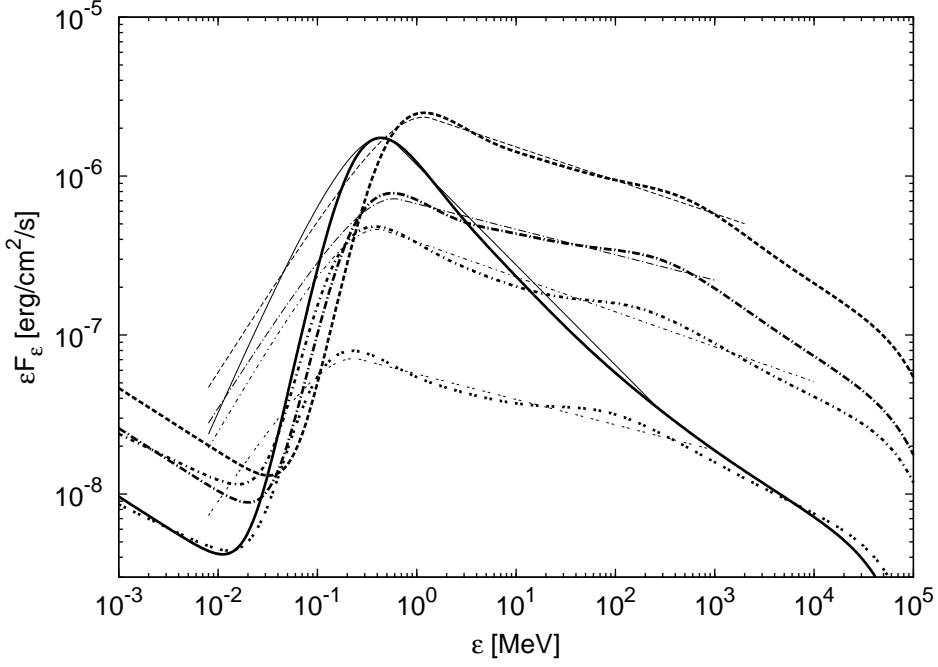


**Figure 3.** Model fits of the time-resolved spectra of GRB 080916C. The thin lines are the observed data, and the thick lines are the model fits (solid lines are for 0.0 – 3.6 s, dashed lines are for 3.6 – 7.7 s, dot-long-dashed lines are for 7.7 – 15.8 s, dot-short-dashed lines are for 15.8 – 54.7 s, and the two-dot lines are for 54.7 – 100.8 s). Adopted parameter values are listed in Table 2. The spectral portions at and above the peak energies are well described by the model. The observed spectral parts below the peak energies are significantly softer than the model. This issue is discussed in Section 6.

the model parameters,

$$L_{53} \left( \frac{\eta}{\eta_*} \right)^{8/3} \sim 4.5 \left( \frac{L_{\text{ph}}}{4.5 \times 10^{53} \text{ erg s}^{-1}} \right), \quad (32)$$

$$L_{53} \left( \frac{\epsilon_d \epsilon_e}{0.1} \right) \sim 11 h^{-1} \left( \frac{L_{\text{up}}}{1.1 \times 10^{53} \text{ erg s}^{-1}} \right), \quad (33)$$

$$L_{53}^{1/4} \left( \frac{r_{a,7}}{\Gamma_a} \right)^{-1/2} \left( \frac{\eta}{\eta_*} \right)^{8/3} \sim 0.75 \left( \frac{\epsilon_{\text{ph}}}{6.3 \text{ MeV}} \right), \quad (34)$$

$$\mathcal{R}_1^{-1} \left( \frac{\epsilon_d \epsilon_e}{0.1} \right) \sim 0.32 \left( \frac{\gamma_m}{2.6} \right) \left( \frac{f(p)}{1.9} \right)^{-1}, \quad (35)$$

$$L_{53}^{-1/3} \left( \frac{r_{a,7}}{\Gamma_a} \right)^{-2/3} \eta_3^{7/3} \mathcal{R}_1^{2/3} t_{v,-2} \left( \frac{a_L}{5} \right)^{-2} \sim 7.9 \left( \frac{\gamma_c}{20} \right). \quad (36)$$

We can constrain the parameters  $L$ ,  $\eta$ ,  $r_a/\Gamma_a$ ,  $\mathcal{R}$ , and  $t_v$  through these equations, by choosing reasonable values  $\epsilon_d \epsilon_e \sim 0.1$  and  $a_L \sim 5$  for internal shock. The parameters  $\beta_{\text{ph}}$  and  $p$  have already been constrained directly by the model fit. The remaining parameter  $\epsilon_d \epsilon_B$  does not affect the photospheric and UP spectra and it is constrained by the synchrotron emission contribution in the low energy range (see below). The above first three equations (32, 33, and 34) provide  $L_{53} \sim 11 h^{-1}$ ,  $(\eta/\eta_*)^{8/3} \sim 0.41 h$ , and  $r_{a,7}/\Gamma_a \sim 0.98 h^{3/2}$ . We have some allowed ranges of parameters depending on the value of  $\gamma_m$ . For  $\gamma_m \sim 2.6$ , we have  $h \sim 0.98$ , and Equations (35) and (36) lead to  $\mathcal{R} \sim 3$ ,  $\eta_3 \sim 4.9$ , and  $t_{v,-2} \sim 0.2$ , where Equation (2) is used. If we adopt a smaller value, e.g.,  $\gamma_m \sim 1$ , we have  $h \sim 0.45$ , leading to  $\mathcal{R} \sim 8$ ,  $\eta_3 \sim 7.4$ , and  $t_{v,-2} \sim 0.02$ . The synchrotron

emission fluxes, which are dominant below 10 keV, should be smaller than the observed fluxes around 10 keV, which provide upper bounds  $\epsilon_d \epsilon_B \lesssim 0.1$  for both cases. A larger  $h$  case has a smaller luminosity budget  $L$ . Comparisons of the prompt emission with the afterglow in GRBs generally imply high radiation efficiencies of the prompt emission,  $\epsilon_\gamma \gtrsim 0.5$  (e.g., Panaitescu & Kumar 2002). Thus we favor the case of the allowed smallest luminosity, i.e., the case of  $\gamma_m \sim 2.6$ , which we list the constrained parameter values in Table 2.

Next we consider the *first* time-bin spectrum. If the internal shock for this component produces an electron energy distribution with  $p \simeq 2.8$  similar to the second time-bin, the UP emission would have a hard photon index  $-(p+2)/2 \simeq -2.4$  in the GeV energy range. Thus the UP emission has to be very dim compared with the photospheric emission, and the overall spectrum would consist mainly of the photospheric emission. The luminosity ratio should be  $L_{\text{up}}/L_{\text{ph}} = x \lesssim 0.06$ . The internal shock may have  $\epsilon_d \epsilon_e \sim 0.1$  similar to the second time-bin, so that we require  $\eta \gtrsim \eta_*$  (see Equations 18 and 30). Thus this spectrum corresponds to case 9 (see Table 1). As shown by the thick solid line in Figure 3, we can fit the spectrum mainly by the photospheric emission whose luminosity, peak energy, and high-energy spectral index are set to be  $L_{\text{ph}} \sim 3.1 \times 10^{53} \text{ erg s}^{-1}$ ,  $\epsilon_{\text{ph}} \sim 2.3 \text{ MeV}$ , and  $\beta_{\text{ph}} \sim -3.0$ , respectively. Equations (3) determine the parameters  $L$  and  $r_a/\Gamma_a$  by  $L_{\text{ph}}$  and  $\epsilon_{\text{ph}}$ ,  $L_{53} \simeq L_{\text{ph},53} \sim 3$  and  $r_{a,7}/\Gamma_a \sim 20$ . The allowed ranges of  $\eta$ ,  $\mathcal{R}$ , and  $t_v$  are broad since the UP spectrum is not tightly constrained. Equation (31) means that larger  $\eta$  decreases the UP luminosity. The model fit shown in Figure 3 is a case with the maximum contribution of the UP emission, i.e., a case of

**Table 2.** Best fit model parameters for GRB 080916C, GRB 090902B, and GRB 090510

GRB 080916C <sup>a</sup>	Time-bin	$L_{53}$	$r_{a,7}/\Gamma_a$	$\eta_3$	$\mathcal{R}_1$	$\beta_{\text{ph}}$	$t_{v,-2}$	$p$	$\epsilon_d \epsilon_e$	$\epsilon_d \epsilon_B$	$\eta/\eta_*$
	0.0 – 3.6 s	3	20	3.2	2	-3.0	< 1.0	2.8	0.1	< 1	1.6
		3	20	3.1	2	-2.7	0.1	2.8	0.01	< 1	1.6
	3.6 – 7.7 s	10	0.9	4.9	3	-2.5	0.2	2.8	0.1	$\gtrsim 0.1$	0.71
	7.7 – 15.8 s	5	1	3.2	3	-2.5	0.6	2.8	0.1	$\gtrsim 0.1$	0.61
	15.8 – 54.7 s	3	1	2.5	3	-2.5	0.7	2.6	0.1	$\gtrsim 0.1$	0.52
	54.7 – 100.8 s	0.7	2	1.6	3	-2.5	1.5	2.6	0.1	$\gtrsim 0.2$	0.55
<hr/>											
GRB 090902B <sup>a</sup>	Time-bin	$L_{53}$	$r_{a,7}/\Gamma_a$	$\eta_3$	$\mathcal{R}_1$	$\beta_{\text{ph}}$	$t_{v,-2}$	$p$	$\epsilon_d \epsilon_e$	$\epsilon_d \epsilon_B$	$\eta/\eta_*$
	4.6 – 9.6 s	16	2	3.5	3	-4.0	10	2.9	0.1	0.1	0.52
<hr/>											
GRB 090510 <sup>a</sup>	Time-bin	$L_{53}$	$r_{a,7}/\Gamma_a$	$\eta_3$	$\mathcal{R}_1$	$\beta_{\text{ph}}$	$t_{v,-2}$	$p$	$\epsilon_d \epsilon_e$	$\epsilon_d \epsilon_B$	$\eta/\eta_*$
	0.5 – 0.6 s	1	3	73	2	-4.8	0.3	2.3	0.1	< 1	26
		1	3	5.4	2	-4.8	0.1	2.3	$5 \times 10^{-3}$	< 1	1.9
	0.6 – 0.8 s	4	0.3	4.7	2	-3.0	0.2	2.3	0.1	$\gtrsim 7 \times 10^{-3}$	0.72
	0.8 – 0.9 s	20	$2 \times 10^{-3}$	3.8	0.5	-2.8	0.2	2.05	0.15	$\gtrsim 3 \times 10^{-6}$	0.18
		10	0.01	1.6	0.6	-2.5	7	2.15	0.15	$\gtrsim 4 \times 10^{-6}$	0.12

<sup>a</sup> These values are example sets of parameter values for producing the fitting spectra, for which  $L$  is the allowed smallest values for each time-bin. See texts for detailed explanations how to specify the other values. Two sets of the parameter values are shown for the time-bins of 0.0 – 3.6 s of GRB 080916C, 0.5 – 0.6 s and 0.8 – 0.9 s of GRB 090510. The parameter  $a_L$  is taken as 5 for all the time-bins except that we take  $a_L = 2$  for the second set for the 0.0 – 3.6 s time-bin of GRB 080916C and for the second set for the 0.5 – 0.6 s time-bin of GRB 090510.

the minimum  $\eta$  for the fixed values  $\epsilon_d \epsilon_e \sim 0.1$  and  $p \simeq 2.8$ . This model fit requires the luminosity and characteristic energies of the UP emission to be  $L_{\text{up}} \sim 2.0 \times 10^{52}$  erg  $\text{s}^{-1}$ ,  $\epsilon_{\text{up},h} \sim 27$  MeV, and  $\epsilon_{\text{up},l} \lesssim 10$  MeV, respectively (corresponding to  $\gamma_h \sim 3.4$  and  $\gamma_l \lesssim 2.1$ ). Equations (9) and (29) indicate that we can have similar values of the model parameters  $\mathcal{R}$  and  $t_v$  as for the second time-bin, i.e., we have  $\gamma_m \sim 3.4$  and  $\gamma_c \lesssim 2.1$  for  $\mathcal{R}_1 \sim 2.4$  and  $t_{v,-2} \lesssim 1.0$ . Since  $\gamma_c < \gamma_m$ , we have  $h = 1$ , so that Equation (31) provides  $\eta_3 \sim 3.2$ .

Alternatively, we may consider a case of  $\epsilon_d \epsilon_e \ll 0.1$  for the first time-bin. For the case of  $\eta > \eta_*$ , the final Lorentz factors of the shells are given by  $\eta_*$ , which may not be much different, i.e.,  $a_L \lesssim 2$ , since it depends weakly on  $L$ ,  $r_a/\Gamma_a$ , and  $\mathcal{R}$ . Then the internal shocks may only cause a weak dissipation, with  $\epsilon_d \epsilon_e \ll 0.1$ . The observed first time-bin spectrum can be fitted by a photospheric emission only, with  $\beta_{\text{ph}} \simeq -2.7$  in this case. The model parameters  $L$  and  $r_a/\Gamma_a$  are constrained to be the same as the above case  $\epsilon_d \epsilon_e \sim 0.1$ . For  $\epsilon_d \epsilon_e \sim 0.01$  as an example, we can find a set of parameter values  $\eta$ ,  $\mathcal{R}$ , and  $t_v$  similar to those for the second time-bin, which are shown in Table 2.

The spectral shapes of the other three time-bins are very similar to that of the second time-bin. They can also be produced by a combination of the photospheric and UP components in our model, where the luminosity ratios of the two components are required to be relatively large, i.e.,  $x \sim 0.3$ , which indicate case 1, similar to the second time-bin. We can constrain the model parameter values for the three time-bin spectra in a similar way to the second time-bin spectrum. The parameters constrained for the case of the allowed smallest luminosity budgets are summarized in Table 2. The rightmost column represents the value of  $\eta/\eta_*$  calculated for the adopted parameter values.

The  $e^\pm$  pair-creation break energies under the isotropic photon field assumption is given by  $\epsilon_{\gamma\gamma,\text{min}}^{\text{ph}}/(1+z) \sim 10$  GeV for the first time-bin and  $\epsilon_{\gamma\gamma,\text{min}}^{\text{ph}}/(1+z) > 50$  GeV for the other time-bins. Since the target photon field is highly anisotropic, the real break energies may be much larger than those values (see references listed above Equation 23), so that we have neglected the pair-creation breaks in Figure 3. We confirm that the second-order UP emission is negligible for each time-bin. For the second to fifth time-bin spectra, we have  $\eta\gamma_c m_e c^2 \ll \gamma_c^2 \epsilon_{\text{up},c}$ , so that the KN effect suppresses the second-order UP emission. For the first time-bin, the second-order UP emission flux is just much smaller than the other emission components. The parameters satisfy our assumptions of  $r_i \gg r_f$  for the first time-bin (Eq. 25) and  $r_i \gg r_{\text{ph}}$  for the other time-bins (Eq. 8).

We have shown that the parameter regime should shift from  $\eta > \eta_*$  into  $\eta < \eta_*$  to reproduce the observed first and second time-bin spectra in our model. This shift is related to the large decrease of  $r_a/\Gamma_a$  from  $\sim 2 \times 10^8$  cm in the first time-bin to  $\sim 1 \times 10^7$  cm in the second time-bin. At this transition, the luminosity ratio of the photospheric and UP components  $x = L_{\text{up}}/L_{\text{ph}}$  (Equations 30 and 18) increases as  $r_a/\Gamma_a$  decreases (and then  $\eta_*$  increases) and possibly  $\epsilon_d \epsilon_e$  increases because of the increasing differences of the final Lorentz factors of the shells. As we discuss in Section 6, the simulations of the jet dynamics in the progenitor star (Morsony et al. 2007) suggest that  $r_a/\Gamma_a$  may undergo a sudden decrease as time progresses. Thus this transition may be interpreted as the reason for the observed delay of the LAT emission onset. After the transition, the parameter sets constrained for the allowed smallest luminosities indicate that  $L$ ,  $\eta$ , and  $t_v$  evolve monotonically, while  $r_a/\Gamma_a$ ,  $\mathcal{R}$ ,  $\beta_{\text{ph}}$ , and  $p$  are stable (note that the values of  $\epsilon_d \epsilon_e$  and  $a_L$  are given to determine the other parameters).

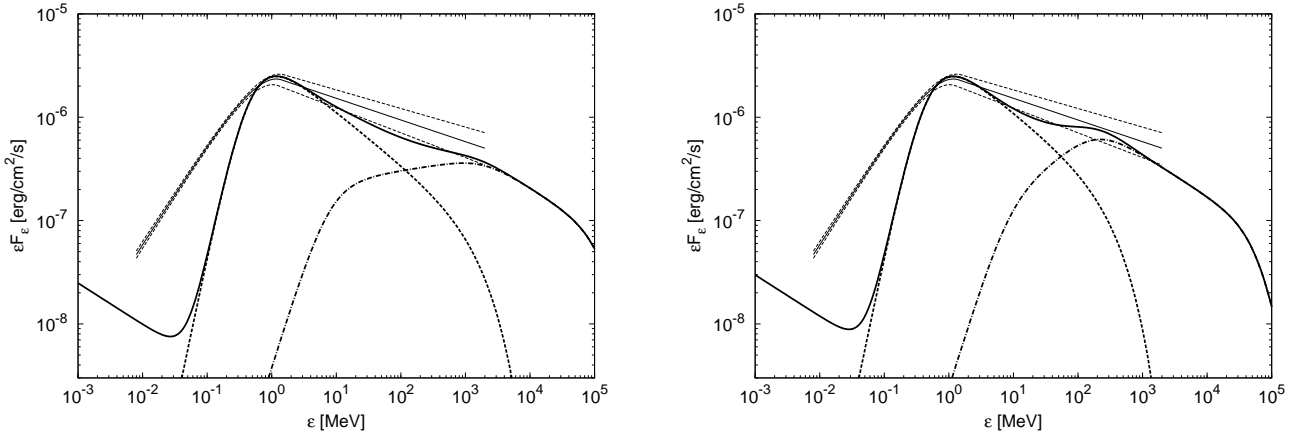


**Figure 4.** Model spectra for the second time-bin spectrum of GRB 080916C, for different values of  $t_v$  and  $\mathcal{R}$  and fixed values of  $L$ ,  $r_a/\Gamma_a$ ,  $(\eta/\eta_*)^{8/3}$ ,  $\beta_{\text{ph}}$ ,  $p$ ,  $\epsilon_d\epsilon_e$  and  $\epsilon_d\epsilon_B$  as shown in Table 2. Left: The thick solid line is the model spectrum using the best fit parameter values shown in Table 2 except for taking  $t'_v = 2t_v$ , which is compared with the thin lines of the Band function fitting the observed data, with the dashed lines showing the  $1\sigma$  errors (Abdo et al. 2009b). Right: The thick solid line is the model spectrum using the best fit parameter values shown in Table 2 except for taking  $\mathcal{R}' = \mathcal{R}/5$ , which is compared with the same observed data as the Left panel. In both panels the thick dashed lines and the thick dot-dashed lines represent the photospheric and UP components, respectively.

The variability timescale is as small as  $t_v \sim 10^{-3}$  s, which is larger than the light crossing timescale across a Schwarzschild black hole of mass  $\sim 10 M_\odot$ ,  $\sim 10^{-4}$  s. Such a timescale ( $t_v(1+z) \sim 5$  ms in the observer-frame) may not be resolved by the  $\gamma$ -ray detectors that observed this burst as far as we know. The most sensitive detector among them for the 100 keV – 30 MeV range is INTEGRAL, which has a resolution down to 50 ms and found a variability timescale  $\sim 100$  ms (Greiner et al. 2009). An unsteady mass accretion from a convectively unstable torus onto the central compact object might produce such a large timescale of the flux change (Sekiguchi & Shibata 2010), or the interaction of the jet with the stellar envelope could induce a variability with light crossing timescale from the side to the axis of the jet  $\sim R_*\theta_j(1+z)/c \sim 100 (R_*/5 \times 10^{10} \text{ cm})(\theta_j/0.01)$  ms, where  $R_*$  is the stellar radius and  $\theta_j$  is the opening angle of the jet (Morsony et al. 2010).

As seen in Figure 3, the low-energy portions of the spectra of the photospheric emission are much harder than the observed spectral portions below the peak energies. This is currently a generic problem for all photospheric mission models, which will be discussed in Section 6.

Interestingly, the observed peak energies and peak  $\epsilon F_\epsilon$  fluxes in the second to fifth time-bins are clearly consistent with the famous peak energy-luminosity relation (so-called Yonetoku relation; Yonetoku et al. 2004; Ghirlanda et al. 2005, 2010), which implies  $\epsilon_{\text{ph}} \propto L_{\text{ph}}^{1/2}$  in our model. This translates into a relation  $\eta \propto L^{7/16}(r_a/\Gamma_a)^{1/8}\mathcal{R}^{1/4}$  by Equations (4). Considering that  $r_a/\Gamma_a$  and  $\mathcal{R}$  are not much changed in our results and the dependences in the relation are weak, the dominant relation should be  $\eta \propto L^{7/16}$  (or roughly  $\eta \propto L^{1/2}$ ). A degree of fine tuning appears needed to satisfy this relation; this is similar to other GRB emission models, which also require fine tunings of the parameters of the jet (e.g., Ghirlanda et al. 2010; Rees & Mészáros 2005; Thompson et al. 2007; Ioka 2010).

Furthermore, we should clarify how tightly the parameter values related to the UP component are constrained for reproducing the smooth Band-like spectrum by a su-

perposition of the two components for each time-bin. Taking the second time-bin as an example, we make different model spectra by fixing  $L$ ,  $r_a/\Gamma_a$ ,  $(\eta/\eta_*)^{8/3}$ , and  $\beta_{\text{ph}}$  to have the same photospheric component, while changing the other parameters to see whether we obtain a smooth Band-like spectrum. The left model in Figure 4 is the result for a value of  $t_v$  that is 2 times larger than the value in Table 2, which is marginally consistent with the data at  $1\sigma$  level. Even larger  $t_v$ , which leads to larger  $\gamma_c$  (and then larger  $\epsilon_{\text{up},c}$  and smaller  $h$ ), makes the UP component dimmer and then the overall spectrum significantly deviates from the data. We also examine models for smaller  $\mathcal{R}$ , which leads to smaller  $\gamma_c$  (with larger  $\gamma_m$ ). This case keeps  $h \sim 1$  (and then  $L_{\text{up}} = L\epsilon_d\epsilon_e h \sim \text{const.}$ ), making the overall model spectrum somewhat bumpy. For a value of  $\mathcal{R}$  that is 2 times smaller than the value in Table 2, the bumpy model spectrum is marginally consistent with the data at  $1\sigma$  level at  $\epsilon/(1+z) < 1$  GeV but does not reproduce the flux at  $\epsilon/(1+z) > 1$  GeV because of smaller  $\epsilon_{\text{up},c}$ . Even smaller  $\mathcal{R}$  leads to the fast-cooling case  $\gamma_c < \gamma_m$ . The spectrum below the UP peak energy is harder than the slow-cooling case with  $p \simeq 2.8$ , so that the model spectrum is more bumpy, although a higher  $\epsilon_{\text{up},m}$  can explain the emission at the high-energy range. The right model in Figure 4 is the result for a value of  $\mathcal{R}$  that is 5 times smaller than the value in Table 2, which is still marginally consistent with the data at  $1\sigma$  level. For a smaller  $\mathcal{R}$ , however, the overall model spectrum significantly deviates from the data in the middle range  $\sim 10$  MeV – 1 GeV. This parametric study indicates that the parameter spaces of  $t_v$  and  $\mathcal{R}$  are limited within a factor of  $\sim$  a few for obtaining a Band-like function by the superposition of the two components.

This means that in order to obtain the Band-like spectra through the second to fifth time-bins, we need significant fine tuning of the model parameters  $t_v$  and  $\mathcal{R}$  (as well as  $\beta_{\text{ph}}$  and  $p$ ). However, we note that Abdo et al. (2009b) conclude “Compared to the null hypothesis that the data originated from a simple Band GRB function, adding the additional power-law component resulted in a probability of 1% that

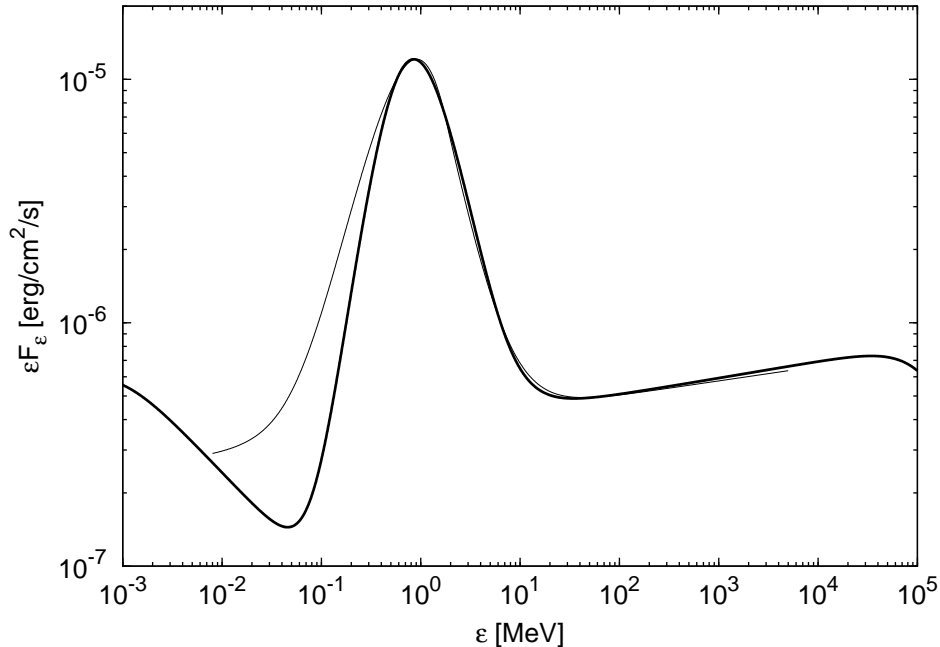


**Figure 5.** Model fit of the spectrum of GRB 090902B in the 4.6 – 9.6 s time bin. The thin line is the observed data, and the thick line is the model fit. Adopted parameters are listed in Table 2. The photospheric and UP emission components are consistent with the observed spectra of the Band component at and above the peak energy and the distinct high-energy power-law component, respectively. The observed low-energy spectrum of the Band component is softer than the model. This issue is discussed in Section 6. A deviation from the Band component at  $\lesssim 40$  keV could be explained by a contribution from the synchrotron component.

there was no additional spectral component for this (fourth) time bin.” Taken at face value, this would imply that the fourth time-bin data may have an additional high-energy spectral component besides the Band function although the significance level is low ( $\sim 2\sigma$  level). Furthermore, the light curve at  $< 10^3$  s in Abdo et al. (2009b) shows the abrupt steepening break of the GBM light curve at the fifth time-bin while the LAT flux decays stably, which implies a two component origin at this time-bin. Zhang et al. (2010) claim that the background uncertainty significantly affect the results of the spectral analysis due to the low count rate at such late times. These implications increase the plausibility of our two component model.

## 5.2 GRB 090902B

This burst is a long GRB that occurred at a redshift  $z \simeq 1.82$  (which corresponds to  $d_L \simeq 4.3 \times 10^{28}$  cm). The results of the time-resolved spectral analysis by Abdo et al. (2009c) show that all the spectra can be fitted by a Band function plus a distinct power-law function. They did not list the flux normalizations of the two components and only show an overall spectrum for the second time-bin 4.6–9.6 s, which we show by the thin line in Figure 5. We apply our model only for this time-bin spectrum. The LAT emission starts  $\sim 3$  s after the GBM trigger within the first time-bin 0.0 – 4.6 s. The delay time in the cosmological rest frame is  $\sim 3/(1+z)$  s  $\sim 1$  s, which is similar to that of GRB 080916C.

The Band and distinct high-energy power-law components of the second time-bin spectrum can be straightforwardly modeled by the photospheric and UP emission, re-

spectively, as shown by the thick line in Figure 5. The observed data of *Fermi*/GBM show a clear deviation from the Band function at  $\lesssim 40$  keV, and the thin line is obtained by assuming that the low-energy excess and the high-energy emission at  $\gtrsim 50$  MeV are the same power-law emission component (Abdo et al. 2009c). In our model, however, the low-energy excess could be a contribution from the synchrotron component, which is separate from the high-energy UP component. If the superposition of the multiple photospheric emission from different shells can reproduce the observed low-energy power-law portion of the Band component (see Section 6 for more discussion) and it extends even below  $\sim 40$  keV, the contribution from the synchrotron component could explain the observed low-energy excess. The model fit is obtained by setting the conditions  $L_{\text{ph}} \sim 2.8 \times 10^{53}$  erg s $^{-1}$ ,  $\epsilon_{\text{ph}} \sim 2.4$  MeV,  $\beta_{\text{ph}} \sim -4.0$ ,  $L_{\text{up}} \gtrsim 1.3 \times 10^{52}$  erg s $^{-1}$ ,  $\epsilon_{\text{up,c}} \gtrsim 40$  GeV,  $\epsilon_{\text{up,m}} \lesssim 16$  MeV, and  $p \sim 2.9$  (which correspond to  $\gamma_c \gtrsim 130$  and  $\gamma_m \lesssim 2.6$ ). For these values we have  $L_{\text{up}}/L_{\text{ph}} = x \gtrsim 0.06$ , and  $h = (\gamma_c/\gamma_m)^{2-p}/(3-p) \lesssim 0.2$ . These lead to  $\eta < \eta_*$  for a reasonable assumption of  $\epsilon_d \epsilon_e \lesssim 0.1$ , and thus this spectrum corresponds to case 1, similar to the second time-bin of GRB 080916C. From these conditions and given values  $\epsilon_d \epsilon_e \sim 0.1$  and  $a_L \sim 5$ , we can constrain the model parameter values, in a similar way to that for GRB 080916C. A larger  $h$  (for a smaller  $\gamma_c$  and a larger  $\gamma_m$ ) leads to the smaller luminosity  $L$ , while in order to explain the low-energy excess as the synchrotron emission at  $\epsilon > \epsilon_{\text{syn,c}}$  with a reasonable range  $\epsilon_d \epsilon_B \lesssim 0.1$ , we require  $\gamma_c \gtrsim 350$  (for which  $L_{\text{up}} \gtrsim 1.6 \times 10^{52}$  erg s $^{-1}$  is needed to explain the high-energy emission). In Table 2, we show the parameter

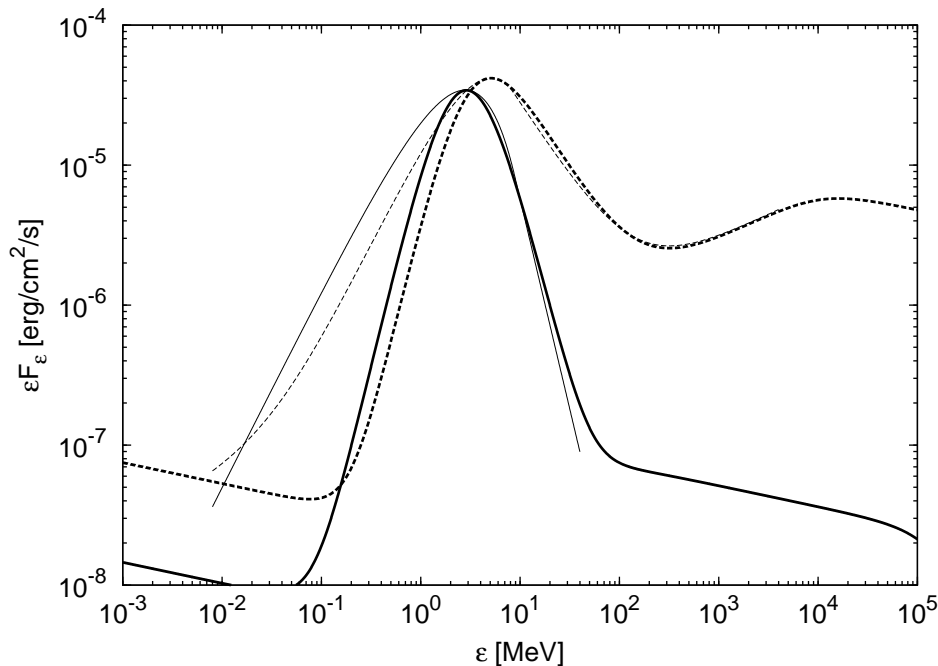


**Figure 6.** Model fits of the time-resolved spectra of GRB 090510. The thin lines are the observed data, and the thick lines are the model fits (the solid lines are for 0.5 – 0.6 s, and the dashed lines are for 0.6 – 0.8 s). Model parameter values are listed in Table 2. The observed spectral parts below the peak energies are significantly softer than the model. This issue is discussed in Section 6.

sets constrained for the case of  $\gamma_c \sim 350$ ,  $\gamma_m \sim 2.6$ , and  $L_{\text{up}} \sim 1.6 \times 10^{52}$  erg s $^{-1}$ . They satisfy our assumption of  $r_i \gg r_{\text{ph}}$  (Eq. 8). The internal shock region is found to be optically thin for  $e^\pm$  pair creation. The second-order UP emission is confirmed to be negligible.

It has been reported that the Band component of this burst can be fitted by a multi-temperature blackbody spectrum (Ryde et al. 2010). The observed low-energy spectral slope of the Band component  $\alpha \simeq 0.07$  is relatively hard and near (but still softer than) the single-temperature thermal model  $\alpha_{\text{ph}} = 1$ , and the high-energy spectral slope  $\beta \simeq -3.9$  is very steep. These strongly favor a photospheric origin of the Band component of this burst.

The first time-bin of GRB 090902B includes a very small number of the high-energy photons, which implies larger  $\eta/\eta_*$ . Thus the LAT onset delay in this burst may be consistent with the interpretation that the parameter regime shifts from  $\eta > \eta_*$  in the first time-bin into  $\eta < \eta_*$  in the second time-bin, similar to the case of GRB 080916C.

### 5.3 GRB 090510

This burst is a short GRB that occurred at a redshift  $z \simeq 0.90$  (corresponding to  $d_L \simeq 1.8 \times 10^{28}$  cm). This has a precursor  $\sim 0.5$  s earlier than the main burst. The analysis results of four time-binned spectra of the main burst are given in Ackermann et al. (2010a). The first and second time-bin spectra are shown by the thin lines in Figure 6, and the third time-bin spectrum in Figure 7. The first time-bin spectrum can be fitted by a Band function only, while the second and third time-bin spectra can be fitted by Band plus distinct power-law functions. For the last time-bin 0.9 – 1.0 s, the emission was detected only in

the LAT energy range (100 MeV – 2 GeV), whose spectrum is fitted by a power-law function. We will not fit this last time-bin spectrum with our model but we discuss a possible explanation for it in the context of our model. The onset delay of the distinct high-energy component with respect to the Band component in the cosmological rest frame is estimated to be  $\sim 0.1/(1+z)$  s  $\sim 0.05$  s. It is remarkable that the distinct high-energy component is brighter than the Band component in the third time-bin, which is unique among all the observed LAT GRBs.

We first consider the *second* time-bin spectrum. This may be explained by a combination of the photospheric and UP emission components. The model parameters for this spectrum can be found in a similar way to the case of GRB 090902B. The luminosity ratio is required to be  $L_{\text{up}}/L_{\text{ph}} = x \gtrsim 0.1$ , and we estimate that  $h \lesssim 0.7$ . These lead to  $\eta \lesssim \eta_*$  for a reasonable assumption  $\epsilon_d \epsilon_e \lesssim 0.1$ , and thus this spectrum corresponds to case 1, similar to the second time-bins of GRB 080916C and GRB 090902B. The best fit model for this spectrum is shown by the thick dashed line in Figure 6, for which  $L_{\text{ph}} \sim 1.7 \times 10^{53}$  erg s $^{-1}$ ,  $\epsilon_{\text{ph}} \sim 9.7$  MeV,  $\beta_{\text{ph}} \simeq -3.0$ ,  $L_{\text{up}} \gtrsim 2.3 \times 10^{52}$  erg s $^{-1}$ ,  $\epsilon_{\text{up},c} \gtrsim 20$  GeV,  $\epsilon_{\text{up},m} \lesssim 44$  MeV, and  $p \simeq 2.3$  are required. From these conditions and given values  $\epsilon_d \epsilon_e \sim 0.1$  and  $a_L \sim 5$ , we can constrain the model parameter values in a similar way to the cases for GRB 080916C and GRB 090902B. The parameter sets constrained for the allowed smallest luminosity (i.e., for  $\epsilon_{\text{up},c} \sim 20$  GeV,  $\epsilon_{\text{up},m} \sim 44$  MeV, which lead to the largest  $h$ , and  $L_{\text{up}} \sim 2.3 \times 10^{52}$  erg s $^{-1}$ ) are shown in Table 2.

Next we consider the *first* time-bin spectrum. This should be produced by the photospheric emission only and the luminosity ratio is required to be  $L_{\text{up}}/L_{\text{ph}} = x \lesssim 3 \times 10^{-3}$ . For a reasonable value  $\epsilon_d \epsilon_e \sim 0.1$ , we have  $\eta > \eta_*$ .

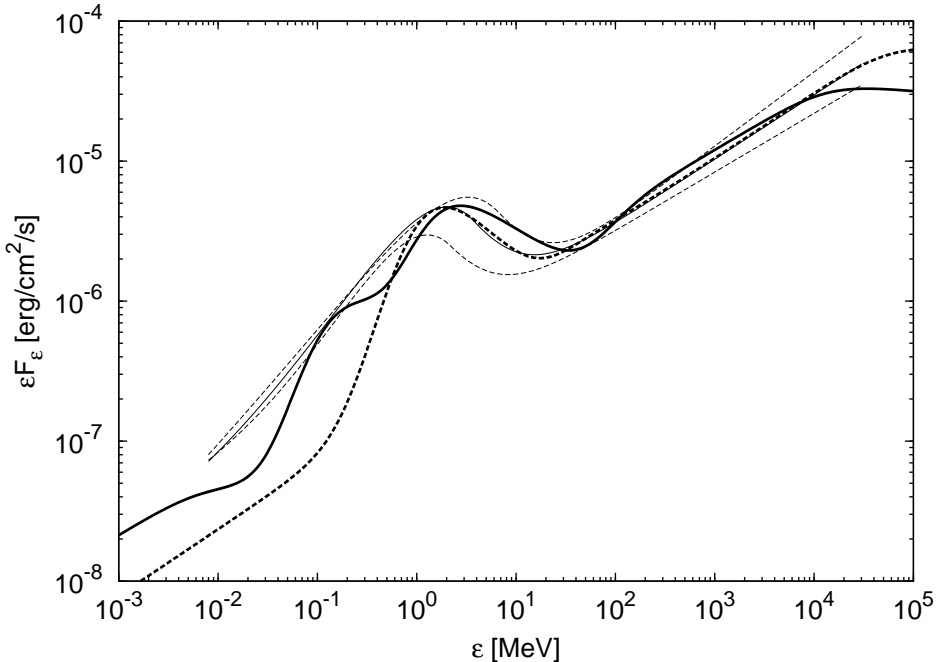


**Figure 7.** Model fits of the third time-bin (0.8 – 0.9 s) spectrum of GRB 090510. The thin line is the Band plus power-law function fitting to the observed data and the thin dashed lines represent the  $1\sigma$  errors. The thick solid and dashed lines are our model fits. Model parameter values are listed in Table 2. See texts for details.

This spectrum corresponds to case 9 (see Table 1). The model fit shown by the thick solid line in Figure 6 requires that the photospheric emission has  $L_{\text{ph}} \sim 1.4 \times 10^{53} \text{ erg s}^{-1}$ ,  $\varepsilon_{\text{ph}} \sim 5.5 \text{ MeV}$ , and  $\beta_{\text{ph}} \sim -4.8$ . Equations (3) determine  $L_{53} \simeq L_{\text{ph},53} \sim 1$  and  $r_{a,7}/\Gamma_a \sim 3$ . These lead to a very large  $\eta/\eta_* \simeq L\epsilon_d\epsilon_e h/L_{\text{up}} \sim 30(\epsilon_d\epsilon_e/0.1)$ , indicating a very large  $\eta \sim 10^5$ . The parameters for the model fit shown in Figure 6 are shown in Table 2.

We can also consider a case of  $\eta > \eta_*$  and  $\epsilon_d\epsilon_e \ll 0.1$  for the first time-bin, similar to the first time-bin of GRB 080916C. We show a result for a case of  $\epsilon_d\epsilon_e \sim 5 \times 10^{-3}$  in Table 2, in which  $\eta/\eta_* \sim 2$  and  $\eta \simeq 5.4 \times 10^3$ . In this case Equation (9) provides  $\gamma_m \sim 0.1 < 1$ , which means in reality that most of the leptons have  $\gamma \sim 1$  and only a small fraction  $\sim 0.1$  of them participate in the non-thermal power-law acceleration. The UP component spectrum has a bump around  $\varepsilon_{\text{ph}}$ , which makes a small contribution to the overall spectrum.

Next we find the parameter values appropriate for the third time-bin spectrum. In this time-bin the UP luminosity has to be higher than the photospheric luminosity. This may correspond to case 2 (see Table 1), unlike the cases considered above. The spectrum can be fitted as shown by the thick dashed line in Figure 7, where the emission component at  $\varepsilon/(1+z) < 0.1 \text{ MeV}$  is the SSC emission (the second-order SSC emission is hidden by the UP emission). The characteristic quantities required for this model fit are  $L_{\text{ph}} \sim 1.8 \times 10^{52} \text{ erg s}^{-1}$ ,  $\varepsilon_{\text{ph}} \sim 3.6 \text{ MeV}$ ,  $\beta_{\text{ph}} \simeq -2.8$ ,  $L_{\text{up}} \gtrsim 2.3 \times 10^{53} \text{ erg s}^{-1}$ ,  $\varepsilon_{\text{up},c} \gtrsim 100 \text{ GeV}$ ,  $\varepsilon_{\text{up},m} \lesssim 50 \text{ MeV}$ , and  $p \simeq 2.05$ . For a somewhat larger  $\epsilon_d\epsilon_e \sim 0.15$ , we can constrain the model parameter values in a similar way to case 1, and the results are shown in Table 2. The value  $r_{a,7}/\Gamma_a \sim 2 \times 10^{-3}$  is much smaller than that in the second

time-bin. This leads to  $r_a \gtrsim 2 \times 10^4 \text{ cm}$ , which is too small, compared to a Schwarzschild radius  $\sim 3 \times 10^5 \text{ cm}$  of the central compact object of mass  $\sim M_\odot$ . If we take a smaller  $L_{\text{up}}$  and  $\varepsilon_{\text{up},c}$  which are consistent with the data at  $1\sigma$  level, i.e.,  $L_{\text{up}} \sim 1.2 \times 10^{53} \text{ erg s}^{-1}$  and  $\varepsilon_{\text{up},c} \sim 25 \text{ GeV}$ , we have  $r_a/\Gamma_a \sim 6 \times 10^4 \text{ cm}$  (and we have  $L_{53} \sim 10$  smaller than the larger  $L_{\text{up}}$  model). At such a late phase of the prompt emission, the external shock emission might contribute to the high-energy emission (De Pasquale et al. 2010), but this possibility is suggested to be unlikely (He et al. 2010) (see also Liu & Wang 2010). Below we show another sets of parameter values which could explain the third time-bin emission at  $1\sigma$  level together with the fourth time-bin emission, and have an even larger  $r_a/\Gamma_a$ .

Finally we discuss the fourth time-bin spectrum. In this time-bin, only the high-energy photons are detected, which requires much larger  $\epsilon_d\epsilon_e$  and/or much smaller  $r_a$ . These do not seem realistic. Here we show an example of another parameter set for the *third* time-bin spectrum, for which the duration of the UP emission can be larger than the pulse width of the MeV photospheric emission and stays bright even in the fourth time-bin without the MeV emission. Here we consider the inefficient scattering regime for the third time-bin (see Section 3; we have assumed the efficient scattering regime for the first and second time-bins, say a case of  $\tilde{W} \sim c\tilde{t}_v$ ), in which the widths of the two shells  $W$  are not much different from those for the earlier time-bins  $\tilde{W}$ , but the separation of the two shells  $ct_v$  is much larger than those for the earlier time-bins  $c\tilde{t}_v$ . In this regime we consider a case of  $a_L^{-2}ct_v \sim W + c\tilde{t}_v \sim 2c\tilde{t}_v$ , for which the leptons in the internal shock of the given two shells with  $W$  and  $t_v$  up-scatter the photospheric emission from a third shell at a distance  $c\tilde{t}_v$  behind these two shells. In this case the angular

spreading timescale of the UP emission is estimated to be  $\sim 3a_L^{-1}t_v$ , which is much larger than  $W/c$  and  $t_v$ , so that we have  $\delta t_{\text{up}} \sim 3a_L^{-1}t_v$  (see Eq. 7). Since  $\delta t_{\text{ph}} \sim W/c$ , which means that the UP emission can last much longer than the MeV emission. If  $\delta t_{\text{up}}(1+z)$  is comparable or larger than the duration of the time-bin, 0.1 s, this scenario could explain the fourth time-bin spectrum. Below we show that the model fit of the third time-bin spectrum in this scenario provides a  $t_v$  consistent with the above temporal conditions.

We interpret the observed Band and distinct high-energy components in the third time-bin as the photospheric emission of the third shell and the UP emission produced by up-scattering of the photospheric emission of the third shell by the internal shock of the first and second shells, respectively. The model fit is shown by the thick solid line in Figure 7, which is marginally consistent with the data at  $1\sigma$  level. The photospheric emission of the third shell has  $\tilde{L}_{\text{ph}} \sim 1.8 \times 10^{52} \text{ erg s}^{-1}$ ,  $\tilde{\varepsilon}_{\text{ph}} \sim 5.5 \text{ MeV}$ , and  $\tilde{\beta}_{\text{ph}} \simeq -2.5$ . (Hereafter a tilde denotes a quantity of the third shell.) The UP emission is required to have  $L_{\text{up}} \simeq L\epsilon_d\epsilon_e h \sim 1.2 \times 10^{53} \text{ erg s}^{-1}$ ,  $\varepsilon_{\text{up},c} \simeq \tilde{\varepsilon}_{\text{ph}}\gamma_c^2 \sim 25 \text{ GeV}$ ,  $\varepsilon_{\text{up},m} \simeq \tilde{\varepsilon}_{\text{ph}}\gamma_m^2 \sim 180 \text{ MeV}$ , and  $p \simeq 2.15$ . The condition for  $L_{\text{up}}$  gives us  $L_{53} \sim 10$  for a given  $\epsilon_d\epsilon_e \sim 0.15$ . The photospheric flux of the second shell should be lower than the observed flux level. We take  $L_{\text{ph}} \sim 3.5 \times 10^{51} \text{ erg s}^{-1}$  and  $\varepsilon_{\text{ph}} \sim 0.5 \text{ MeV}$  which produces the spectral bump below the peak energy of the main photospheric emission in Figure 7 and requires  $r_{a,7}/\Gamma_a \sim 0.01$  and  $(\eta/\eta_*)^{8/3} \sim 4 \times 10^{-3}$  through Equation (4). Equation (9) leads to  $\mathcal{R}_1 \sim 0.6$ . Then we have  $\eta_{*,3} \sim 13$  and  $\eta_3 \sim 1.6$ . Finally the remaining parameter  $t_v$  is determined by an equation for  $\gamma_c$ , which is given by Equation (19) multiplied by a factor  $L_{\text{ph}}/\tilde{L}_{\text{ph}} \sim 0.2$ . This factor leads to  $t_{v,-2} \sim 7$ , much larger than in the above simple two-shell scenario. The observed duration of the UP emission pulse is then estimated to be  $\delta t_{\text{up}}(1+z) \sim 3a_L^{-1}t_v(1+z) \sim 0.08 \text{ s}$ . This is comparable to the durations of the third and fourth time-bins and roughly consistent with the condition  $a_L^{-2}ct_v \sim 2\tilde{c}t_v$ , so that the high-energy emission without a corresponding MeV emission in the fourth time-bin could be explained by the UP emission with large angular spreading time.

The value  $r_a/\Gamma_a \sim 10^5 \text{ cm}$  is comparable but still somewhat smaller than a Schwarzschild radius of mass  $\sim M_\odot$ . A larger  $r_a/\Gamma_a$  would lead to a brighter spectral bump of the photospheric emission from the second shell at  $\sim 0.1 \text{ MeV}$  in Figure 7, as  $L_{\text{ph}} \propto (r_a/\Gamma_a)^{2/3}$  and  $\varepsilon_{\text{ph}} \propto (r_a/\Gamma_a)^{1/6}$  in Eq. (4), violating the observed data. This might suggest that a large fraction of the jet energy at  $r_a$  is not thermal but Poynting flux for this burst (cf. Zhang & Pe'er 2009).

To summarize this scenario, the pulse widths of the UP component  $\delta t_{\text{up}} \sim W/c + 3a_L^{-1}\tilde{t}_v$  are similar to those of the photospheric component  $\delta t_{\text{ph}} \sim W/c$  (as  $\sim 1 \text{ ms}$ ) at the first and second time-bins, while at the third time-bin the UP pulse width only increases significantly to  $\delta t_{\text{up}} \sim 3a_L^{-1}t_v \sim 40 \text{ ms}$ , which may stay bright even at the fourth time-bin. This may be consistent with the results of the cross-correlation function analysis by Ackermann et al. (2010a) that there is no correlated variability between the GBM and LAT emission.<sup>4</sup> In this scenario there should be a large in-

terval  $t_v(1+z) \sim 0.1 \text{ s}$  of the photospheric emission before the third time-bin, which seems consistent with the observed quiescent time in the 260 keV – 5 MeV light curve. Such a variability timescale  $\sim 0.1 \text{ s}$  might arise from the mass accretion on the central compact object from an inhomogeneous torus (Rosswog 2007) or from the interaction of the jet with the dense environment (Morsony et al. 2010).

The parameter sets we found for the three time-bin spectra are summarized in Table 2. We have shown that the parameter regime should shift from  $\eta > \eta_*$  in the first time-bin into  $\eta < \eta_*$  in the second time-bin, which is related to the large decrease of  $r_a/\Gamma_a$  and corresponds to the increase of the luminosity ratio  $x = L_{\text{up}}/L_{\text{ph}}$  and the delayed onset of the distinct high-energy component, similar to the cases of GRB 080916C and GRB 090902B. The second and third time-bin spectra satisfy the relation  $\varepsilon_{\text{ph}} \propto L_{\text{ph}}^{1/2}$ , similar to the case of GRB 080916C, which requires a fine tuning of the parameters  $L$ ,  $r_a/\Gamma_a$ ,  $\eta$ , and  $\mathcal{R}$ .

The synchrotron and SSC fluxes should be lower than the observed flux levels, which put constraints on  $\epsilon_d\epsilon_B$ , which is much tighter than the cases of GRB 080916C and GRB 090902B. In particular for the third time-bin, we need  $\epsilon_d\epsilon_B \lesssim 3 \times 10^{-6}$ . A typical value  $\epsilon_d \sim 0.25$  leads to a constraint  $\epsilon_B \lesssim 10^{-5}$ . This is not implausible since some external shocks driven by GRBs have been suggested to have such small values of  $\epsilon_B$  (Panaitescu & Kumar 2002; Granot & Guetta 2003; Pe'er & Waxman 2004). The internal shock region is estimated to be optically thin for the  $e^\pm$  pair creation for the second and third time-bins, and we find  $\varepsilon_{\gamma,\text{ph}}^{\text{min}}/(1+z) \sim 100 \text{ GeV}$  for the first time-bin. The parameter sets for all the time-bins satisfy our assumptions of Equations (8) and (25). The second-order UP emission is negligible for all the time-bins.

## 6 SUMMARY AND DISCUSSION

GRB jets are thought to consist of many successive shells moving at relativistic speeds. These naturally lead to variable photospheric emission around the MeV energy range, and also to internal shocks above the photosphere. Energy dissipation near the photosphere caused by e.g., internal shocks, excited plasma waves, and/or interaction of the jet with the dense environment, or nuclear collisions between protons and neutrons is expected to make the photospheric emission having the power-law tail spectrum above the peak energy  $\varepsilon_{\text{ph}}$ , with the photon index  $\beta_{\text{ph}} \lesssim -2.5$  under the assumption of the roughly adiabatic evolution of the jet (see Section 2). We have generically studied the temporal and spectral properties of the radiation from the photosphere and the internal shock in the jet which is accelerated by

sion correlated with GBM pulses throughout the whole prompt phase. This may not be inconsistent with our second (large  $\delta t_{\text{up}}$ ) scenario for the third time-bin, since the third time-bin model spectrum indicates that the high-energy tail part of the photospheric emission which has sharp variability contributes to  $\sim 50\%$  of ( $\sim 10\%$  of) the observed photon numbers at the entire LAT range  $\gtrsim 20 \text{ MeV}$  (at  $> 100 \text{ MeV}$ ). Also, the UP emission comes from a large area of the shell with solid angle of  $\lesssim 3/\Gamma$  (see Section 3), which could have angular inhomogeneity leading to the sharp variability at the both third and fourth time-bins.

<sup>4</sup> Nevertheless, we can see some narrow spikes of the LAT emis-

the thermal pressure. We have not considered acceleration by processes related to magnetic fields. We have shown that the photospheric emission is efficiently up-scattered to the high-energy range by the electrons (and positrons) accelerated in the internal shocks, for the efficient scattering regime ( $\Gamma_s^2/\Gamma_r^2)t_v < W/2$  which includes the typical case  $W \sim ct_v$  (see Section 3), when the radiation from the internal shocks consist of the UP, synchrotron, and SSC emission components.

Our generic arguments show that the ordering of the luminosities of the emission components depends on the values of  $(\eta/\eta_*)^{8/3}$ ,  $\epsilon_d\epsilon_e h$ , and  $\epsilon_d\epsilon_B$  (see Section 4 and Table 1). A condition  $(\eta/\eta_*)^{8/3} \gg \max(\epsilon_d\epsilon_e h, \epsilon_d\epsilon_B)$  is required in order to have the photospheric and UP components dominant in the MeV energy range and in the high-energy range, respectively, rather than the synchrotron and SSC components, and  $L_{\text{ph}} \gg L_{\text{up}}$  as typically observed in LAT GRBs. (We can also have a case of  $L_{\text{up}} \gg L_{\text{ph}}$  for a condition  $\epsilon_d\epsilon_e h \gg (\eta/\eta_*)^{8/3} \gg [(\epsilon_d\epsilon_e)^2\epsilon_d\epsilon_B]^{1/3}$ , which has been applied to the third time-bin spectrum of GRB 090510.) For reasonable values of  $\epsilon_d\epsilon_e$  and  $\epsilon_d\epsilon_B$  both  $\lesssim 0.1$  for internal shocks, that condition reduces to  $\eta \gtrsim \eta_* \simeq 2.8 \times 10^3 L_{53}^{1/4} (r_{a,7}/\Gamma_a)^{-1/4} \mathcal{R}_1^{1/4}$  (Equation 2). In this case the photospheric emission has luminosities  $L_{\text{ph}} \sim L$ , and its peak energy is given by  $\varepsilon_{\text{ph}} \sim 8 L_{53}^{1/4} (r_{a,7}/\Gamma_a)^{-1/2}$  MeV (Equations 1, 3, and 4), which can be consistent with the Band components of the observed LAT GRBs as well as other GRBs since we can have  $10^{-1} \lesssim r_{a,7}/\Gamma_a \lesssim 10^2$  in principle (but there are several issues to be addressed on the spectral shapes and their temporal evolution; see below). This implies that the GRB jets should typically have a relatively large bulk Lorentz factor at the prompt emission site,  $\sim \eta_*$ , in our model.

The UP emission component is a good candidate for the observed high-energy emission of LAT GRBs in the prompt phase. The long-lived high-energy emission after the prompt phase may be related to the external shock (e.g., De Pasquale et al. 2010; Kumar & Barniol Duran 2010; Ghisellini et al. 2010; He et al. 2010; Liu & Wang 2010). We have performed case studies of the prompt emission of GRB 080916C, GRB 090902B, and GRB 090510, and fitted their time-binned spectra by our model typically with reasonable sets of parameter values (see Section 5 and Table 2). For GRB 090902B and GRB 090510, the UP emission corresponds to the observed distinct high-energy component, while for GRB 080916C, the UP emission is dominant in the high-energy range but the photospheric plus UP emission mimic the Band function between  $\sim 10$  keV and  $\sim 10$  GeV.

We note that fine tuning of the parameter values appears to be required for some spectra in addition to keeping  $\eta \gtrsim \eta_*$ . In order for the combined photospheric and UP components to mimic a simple Band function fit of the spectra of GRB 080916C through the second to fifth time-bins, significant fine tuning of several parameters is required. Such a composite model is, however, compatible with the presence of an additional high-energy component, which is weakly suggested in the data of the fourth time-bin, and also the difference of the temporal behaviors of the GBM and LAT emission suggests a two component origin for the fifth time-bin. Furthermore, the observed spectra of GRB 080916C and GRB 090510 show the temporal evolu-

tion roughly obeying  $\varepsilon_{\text{ph}} \propto L_{\text{ph}}^{1/2}$  from the second time-bins (see also Ghirlanda et al. 2010; Yonetoku et al. 2004), which require a relation  $\eta \propto L^{7/16}$ . For the third and fourth time-bins of GRB 090510, when the distinct high-energy component is much brighter than the Band component, we require an additional shell behind the two colliding shells and besides need  $r_a/\Gamma_a \sim 10^5$  cm close to or even smaller than a Schwarzschild radius of mass  $\sim M_\odot$ ,  $\sim 3 \times 10^5$  cm, and very small  $\epsilon_d\epsilon_B \lesssim 3 \times 10^{-6}$ .

Other LAT GRBs, such as GRB 080825C (Abdo et al. 2009a) and GRB 081024B (Abdo et al. 2010), whose redshifts are not determined, display time-binned spectra fitted by Band functions with a temporal behavior of the high-energy spectral indices  $\beta$  similar to those of GRB 080916C, so that they also may be explained by our model. In our model the UP emission should exist in all GRBs if the jet is in the efficient scattering regime, but for GRBs with small  $L$  this may be below the detection threshold of LAT, since the UP luminosity is proportional to  $L$ . This is a general statement applicable to wide types of models in which  $L$  determines the flux normalizations of both the Band and the high-energy emission components, and consistent with the fact that the high-energy emission is detected by LAT only in the brightest class of *Fermi* GRBs (Granot 2010).

We have shown that if the GRB jet is in the efficient scattering regime right from the start, the simple kinematic effect causes the onset of the first UP emission to be delayed with respect to that of the first photospheric emission by a timescale comparable to the pulse widths or pulse separations of the photospheric emission, which should be smaller than the variability timescale apparent in the MeV light curve (see Section 3). This may not explain the time delays much larger than the apparent variability timescale observed in most of the LAT GRBs. In our model, such observed large time delays may instead be attributed to a temporal evolution of the jet parameters,  $L$ ,  $r_a/\Gamma_a$ ,  $\eta$ ,  $\mathcal{R}$ , and  $t_v$ , a possible origin for which is discussed in the next paragraph. From the model fits of the time-binned spectra of the three LAT GRBs (in Section 5), we found that the parameter regime should shift from  $\eta > \eta_*$  into  $\eta < \eta_*$  to reproduce the observed spectra (this shift leads to the increase of  $L_{\text{up}}/L_{\text{ph}} = x$ ; Equation 18 and 30). In this case the UP emission component starts with a small delay with respect to the photospheric emission onset by the timescale comparable to the photospheric variability time, being still dim compared with the photospheric emission while  $\eta > \eta_*$ , but starts to be bright and detected by LAT when the parameters shift into the regime of  $\eta < \eta_*$ .

This parameter shift appears to be related to the large decrease of  $r_a/\Gamma_a$ , from  $\sim 10^8$  cm to  $\sim 10^7$  cm, in the timescale of  $t_{\text{delay}} \sim 1$  s in long GRBs GRB 080916C and 090902B (Table 2). The progenitors of long GRBs are thought to be collapsing massive stars, and such a decrease of  $r_a/\Gamma_a$  may be explained by the interaction of the jet with the stellar envelope before the jet breakout. The numerical simulations by Morsony et al. (2007) (see also Lazzati et al. 2009) show that the jet has three parts around the time when it breaks out the star; the jet head, the collimation-shocked part, and the free expansion part. The jet head is defined as the very thin part at the front end of the jet between the forward and reverse shocks, which typically has a mildly relativistic speed and the material inside this part es-

capac sideways into the cocoon; a large fraction of the jet behind the jet head, suffering weaker dissipation by collimation shocks, has a relativistic speed; and behind the collimation-shocked part, the jet material suffers much weaker dissipation, expanding adiabatically.<sup>5</sup> For the collimation-shocked part,  $r_a$  may be the stellar radius and  $\Gamma_a$  is given by its Lorentz factor at the breakout time, while for the free expansion part,  $r_a$  may be the size of the central compact object and  $\Gamma_a \sim 1$ . In such a jet structure, the emission properties may be changed at the transition between the collimation-shocked part and the free expansion part. The observed time delay would then correspond to the length scale of the collimation-shocked portion of the jet at the breakout time,  $l_d \sim ct_{\text{delay}} \sim 3 \times 10^{10}$  cm. The radius of this part, which should be slightly larger than  $l_d$ , say  $r_a \sim 5 \times 10^{10}$  cm, could be consistent with the size of the progenitor star and with our spectral modeling if  $\Gamma_a \sim 500$ , which is relativistic but smaller than  $\eta \sim 3 \times 10^3$ . The value  $r_a/\Gamma_a \sim 10^7$  cm for the free expansion part is what might be expected from a compact object size  $r_a \sim 10^7$  cm and  $\Gamma_a \sim 1$ . This  $r_a$  is a few Schwarzschild radii of an object of mass  $\sim 10M_\odot$ . As for the short GRB 090510, the parameter shift appears to be related to the decrease of  $r_a/\Gamma_a$ , from  $\sim 3 \times 10^7$  cm to  $\sim 3 \times 10^6$  cm, on a timescale of  $t_{\text{delay}} \sim 0.1$  s (Table 2). The model fit indicates an even smaller  $r_a/\Gamma_a \sim 10^5$  cm for the third time-bin. This might suggest a smaller size of the progenitor and the central object than those of long GRBs.

In such a scenario, the delay timescale of the LAT emission  $t_{\text{delay}}$  is related to the global properties of the jets and the progenitor systems, rather than the micro-physical processes or the simple kinematic (propagation) effects, and then it might scale with the total duration of the MeV emission  $t_{\text{dur}}$ . However, in our specific model, while  $t_{\text{delay}} \sim f_c R_*/c$  scales with the stellar radius  $R_*$  (where  $f_c$  is the fraction of the collimation-shocked part at the jet breakout),  $t_{\text{dur}}$  may depend on the size of the central region of the star  $R_c$  from which the accretion rate is very high, i.e.,  $t_{\text{dur}} \sim \sqrt{R_c^2/(GM_c)}$ , where  $M_c$  is the mass enclosed within  $R_c$  (cf. Kumar et al. 2008). Then  $t_{\text{dur}}$  may significantly depend on the angular velocity and density profiles of the star, which could not simply scale with  $t_{\text{delay}}$ . Observations of LAT GRBs with redshifts determined show that GRB 080916C, GRB 090902B, and GRB 090926A (Ackermann et al. 2011) have the durations  $t_{\text{dur}} \sim 15$  s,  $\sim 8$  s, and  $\sim 4$  s, respectively, while the delay timescales are all  $t_{\text{delay}} \sim 1$  s. In our scenario  $t_{\text{delay}}$  is expected to be distributed more widely when we obtain a larger number of LAT bursts.<sup>6</sup>

The shift from  $\eta > \eta_*$  into  $\eta < \eta_*$  makes the change of the photospheric luminosity from  $\approx L$  into  $\simeq L(\eta/\eta_*)^{8/3}$ , so that it would decrease if  $L$  was roughly constant. The

observed MeV emission luminosities appear not to decrease (roughly constant for GRB 080916C and GRB 090510 while increase by about a factor of two for GRB 090902B), however, so that  $L$  should increase compensate the shift of the parameter regime of  $\eta/\eta_*$ . Table 2 shows that  $L$  increases from the first to second time-bins by factors of  $\sim 3$  and  $\sim 4$  for GRB 080916C and GRB 090510, respectively, while for GRB 090902B, the increase factor may be estimated to be  $\sim 2/(0.52)^{8/3} \sim 10$ . This may be another parameter tuning required in our model for LAT GRBs, but it might be a selection effect: GRB jets with non-increasing  $L$  could have dim UP emission which is not detected by LAT.

For bursts whose LAT emission stays bright from  $t_{\text{delay}}$  after the trigger, as seen in the three bursts we have studied in detail, the parameter regime is assumed to stay  $\eta < \eta_*$  in a large fraction of the total duration in our model. This means that the radiation efficiencies in those bursts are not so extremely large compared with the photospheric emission models in which  $\eta \gtrsim \eta_*$  is assumed over the total duration. Indeed we can roughly estimate the radiation efficiencies of the three bursts as  $\epsilon_\gamma \sim \Sigma(L_{\text{ph}} + L_{\text{up}})t_{\text{bin}}/\Sigma Lt_{\text{bin}} \sim 0.4$  for GRB 080916C,  $\sim 0.2$  for GRB 090902B, and  $\sim 0.3$  for GRB 090510.<sup>7</sup> Such moderately high efficiencies of prompt emission lead to the external shock emission as bright as the prompt emission, which is consistent with the observations that all the three bursts have bright long-lived high-energy emission. For GRB 090902B, its late-time low-energy afterglow suggests the total isotropic kinetic energy after the prompt phase  $\sim 10^{54}$  erg (Cenko et al. 2010), which is much smaller than estimated from the high-energy afterglow  $\sim 10^{55}$  erg (Kumar & Barniol Duran 2010). This might be attributed to the two-components structure of the jet involving a narrow and bright spot at the line of sight surrounded by a wider and less energetic region (Liu & Wang 2010). Many early X-ray afterglows observed by *Swift* show very steep decays ( $F_\nu \sim t^{-3}$ ), which are not compatible with the bright high-energy afterglows of LAT GRBs, not decaying so rapidly. This is another issue to be solved, and a simultaneous observation by *Fermi*/LAT and *Swift*/XRT from the early times will be very helpful.

The above summary indicates that the photospheric emission models may be viable for the temporal and spectral properties of the MeV and high-energy emission of the *Fermi*/LAT GRBs as well as the other ordinary GRBs, although we need the fine tuning of several parameters (see also the following discussion). Very recently Pe'er et al. (2010) showed detailed simulations of the emission processes at a dissipation region out of the photosphere of the jet in a model similar to ours, including photospheric emission, and concluded that such an emission model can explain the spectrum of GRB 090902B, supporting our rough analytical model. Ioka (2010) explores the emission from the photosphere and internal shock of the jet with a very high  $\eta \sim 10^4 - 10^6$  and argues that the high-energy emission of the LAT GRBs may be explained as synchrotron emission from the internal shock.

<sup>5</sup> For example, Figure 2 of Lazzati et al. (2009) shows that the collimation-shocked part has an averaged Lorentz factor of  $\sim 10^2$  while the free expansion part which follows has a saturated Lorentz factor of  $\eta \sim 400$ .

<sup>6</sup> GRB 090217A displays no delay, i.e.,  $t_{\text{delay}} \sim 0$  s (while  $t_{\text{dur}}(1+z) \sim 33$  s Ackermann et al. 2010b). The earliest LAT emission may be just the detections of the high-energy tail part of the photospheric emission while the UP emission onset could correspond to the second group of the LAT detections at  $> 100$  MeV,  $\sim 7$  s after the burst trigger.

<sup>7</sup> The radiation efficiency of the jet consisting of multiple shells could be enhanced by the cross IC scattering between the shells (e.g., Gruzinov & Mészáros 2000; Li 2010). These effects have not been considered in this paper.

An outstanding problem in the photospheric emission models, including ours is that the low-energy spectrum of the photospheric emission, usually assumed to be the Rayleigh-Jeans part of the blackbody radiation,  $\alpha_{\text{ph}} = 1$ , is much harder than those of the Band components of typical observed GRBs widely distributed around  $\alpha \sim -1$  (Preece et al. 2000; Ghirlanda et al. 2002; Kaneko et al. 2006) as well as those of LAT GRBs shown in Figure 3, 5, 6, and 7. In this paper we have mainly considered the two-shell system like in Figure 1, but the typical duration for the spectral analysis includes many pulses (Note that our model parameters and the analysis time-bins are  $t_v(1+z) \lesssim 0.04$  s and  $T_{\text{bin}} > 3$  s for GRB 080916C,  $t_v(1+z) \sim 0.3$  s and  $T_{\text{bin}} \simeq 5$  s for GRB 090902B, and  $t_v(1+z) \sim 4 \times 10^{-3}$  s and  $T_{\text{bin}} \simeq 0.1$  s for GRB 090510), and thus the superposition of the photospheric emission from the multiple shells with different  $\varepsilon_{\text{ph}}$  has the potential of reproducing the observed low-energy spectrum  $\alpha \ll 1$ .<sup>8</sup> For example, the photospheric emissions from multiple shells with different  $\eta$  and similar  $L$ ,  $r_a/\Gamma_a$ , and  $\mathcal{R}$  have a relation  $L_{\text{ph}} \propto \varepsilon_{\text{ph}}$  (not the conventional blackbody relation  $L_{\text{ph}} \propto \varepsilon_{\text{ph}}^4$ ; see Equation 4), so that their superposition appears as a spectrum  $\varepsilon F_\varepsilon \propto \varepsilon^1$ , i.e.,  $\alpha \sim -1$ .<sup>9</sup> The parameter  $\eta$  should be distributed over a range of a factor  $\sim 5$  to reproduce the low-energy spectrum extending  $\sim 1-2$  decades of energies (Ghirlanda et al. 2007). However this is just a rough speculation, and we need more detailed consistency checks within the model and between the model and observations (see also Mizuta et al. 2010). The spectral analysis of GRBs with  $T_{\text{bin}} \ll 0.1$  s could reveal the intrinsic hard spectrum. Our speculation is not inconsistent with the recent analysis that the spectrum of as small time-bin as  $T_{\text{bin}} \sim 0.5$  s  $\sim t_v(1+z)$  in GRB 090902B becomes close to a blackbody, while the spectra of smaller time-bins but  $T_{\text{bin}} > 5$  s  $\gg t_v(1+z)$  in GRB 080916C keep non-thermal (Zhang et al. 2010; Ryde et al. 2010).

The synchrotron (and SSC) emission models also have a problem with the low-energy spectral index of the Band component. The electrons are required to be cooled so fast that the low-energy spectral slope should be  $\alpha = -3/2$  in simple types of these models (e.g., Ghisellini et al. 2000). This is usually softer than the observed slopes, so that the superposition effect does not work well. There have been many models considering the details of the microphysics in the emission sites, but there is no consensus for this problem yet (e.g., Ghisellini & Celloti 1999; Panaitescu & Mészáros 2000; Medvedev 2000; Derishev et al. 2001; Pe'er & Zhang 2006; Asano & Terasawa 2009; Daigne et al. 2011).

The spectral excesses from the Band component be-

low  $\sim 40$  keV in GRB 090902B could be one of the important discoveries by *Fermi*/LAT, although such an excess was not detected by other detectors extending to sufficiently low energies such as *BeppoSAX* and *HETE-2* (e.g., Ghirlanda et al. 2007) (but see Ryde et al. 2006). If these are real detections, they may be explained in our model as synchrotron or SSC emission from internal shocks, constraining the values of  $\varepsilon_d \varepsilon_B \sim 0.1$  (see Table 2). On the other hand, in order for the synchrotron emission not to be prominent in the low-energy range in GRB 090510, we require  $\varepsilon_d \varepsilon_B \lesssim 7 \times 10^{-3}$  and  $\lesssim 3 \times 10^{-6}$  for the second and third time-bins, respectively. Such a wide range of constrained parameter  $\varepsilon_B$  is similar to the case in the external shock,  $10^{-5} \lesssim \varepsilon_B \lesssim 10^{-2}$ , constrained from the late afterglow observations (Panaitescu & Kumar 2002), but it is one of the fundamental problems for the shock physics to deduce the microphysical parameters  $\varepsilon_B$  as well as  $\varepsilon_e$  and  $p$  from the first principles.

The light curves dominated by the synchrotron or SSC emission should be correlated with those dominated by the UP emission, since they both are produced by the same internal shocks. Such a correlation analysis would be useful to distinguish our photospheric emission model from, e.g., other EIC models (Toma et al. 2009b). If the high-energy emission is produced by up-scattering of soft X-ray emission from an external source, such as a cocoon ejected from a progenitor star, off the electrons in the jet, the light curve of the seed soft X-rays should not be correlated with that of the high-energy component. We note that the kinematic arguments in Section 3 indicate that a fraction of the photospheric emission should also be temporally correlated with the synchrotron, SSC, and UP emission in our model.

The synchrotron component could also be detected in the optical band. For the model parameters for the second time-bin of GRB 090902B shown in Table 2, the synchrotron self-absorption energy in the observer frame is estimated as  $\varepsilon_{\text{syn},a}/(1+z) \sim 7$  eV and then we have a flux  $\sim 320$  mJy at  $3 \times 10^{14}$  Hz, which is a very bright optical source even though it suffers a strong self-absorption. The bright optical prompt emission of some GRBs, being often much brighter than the extrapolation of the Band component (e.g., Briggs et al. 1999; Racusin et al. 2008), could be attributed to the synchrotron emission from the internal shocks in our model.

The spectra of the three LAT GRBs we considered may have spectral breaks at  $\varepsilon_{\text{up},h}$  and at  $\varepsilon_{\text{KN}}$  in the high-energy range, while a break due to the  $e^\pm$  pair creation in the emission site is estimated to be typically much above those breaks in our model. Detecting a spectral break in the high-energy range by *Fermi*/LAT and/or by the future Cherenkov telescope such as CTA<sup>10</sup> would be very helpful to constrain the models.<sup>11</sup> Polarimetric observations of the prompt emission also have the potential of distinguishing the photospheric emission models from the synchrotron emission models (Fan 2009). In the energy range  $\varepsilon \lesssim 1$  MeV, which is the target of some planned missions, the photospheric

<sup>8</sup> The idea of the superposition of the multiple shells emission is similar to a common interpretation of the flat radio spectrum of typical blazars ( $F_\nu \propto \nu^\delta$  with  $\delta \lesssim 0$ ). The radio synchrotron emission is thought to be highly self-absorbed ( $F_\nu \propto \nu^{5/2}$ ), and the emission from the multiple shells can reproduce the observed spectral slope (e.g., Königl 1981; Ghisellini & Tavecchio 2009; Marscher 2009).

<sup>9</sup> Our spectral modeling have suggested that a correlation  $\eta \propto L^{7/16}$  is required in order to reproduce the observed correlation  $\varepsilon_{\text{ph}} \propto L_{\text{ph}}^{1/2}$  in the time-binned spectra of GRB 080916C and GRB 090510 (see Section 5), which should apply for the maximum value of  $\eta$  in some range of times.

<sup>10</sup> <http://www.cta-observatory.org>.

<sup>11</sup> The distinct high-energy power-law component of GRB 090926A has been confirmed to have a spectral break in Ackermann et al. (2011) accepted after the submission of our paper.

emission which consists of the blackbody component and the multiple-scattered blackbody component may have very low polarization, while some of the synchrotron emission models predict detectable degrees of polarization (see also Toma et al. 2009a, for general discussion of GRB polarization).

The case studies in this paper have shown that the photosphere-internal shock model can produce three types of the spectral shapes of GRB prompt emission: (i) The photospheric emission with the high-energy tail of the photon index  $\beta_{\text{ph}} \lesssim -2.5$  makes the Band spectrum up to  $\sim 1 - 10$  GeV while a dim UP emission has a small contribution or just makes the extension of that Band spectrum at  $\gtrsim 1 - 10$  GeV (like the first time-bins of GRB 080916C and GRB 090510); (ii) The UP emission is bright but the combination of the UP and photospheric components mimics a Band function with the high-energy index of  $\beta > \beta_{\text{ph}}$  (like the second to fifth time-bins of GRB 080916C); (iii) The UP emission is bright and makes a high-energy component distinct from a photospheric emission (like the second time-bin of GRB 090902B and the second and third time-bins of GRB 090510). The increasing number of bursts being observed in the LAT field of view (including bursts with no detections in the LAT energy range) will determine the number ratios of the Band-only spectra and the Band plus distinct high-energy component spectra. Extensive parametric studies would then be able to clarify whether our model with reasonably large parameter space is consistent with the high-energy parts of general GRB spectra or only consistent with limited numbers of them. A very recent analysis of 52 bright *Fermi*/GBM bursts ( $\sim 8$  keV – 38 MeV) show that the number of the bursts that can be fitted by a Band function with  $\beta > -2.4$  is 14 ( $\simeq 27\%$ ) and with  $\beta > -2.3$  is 7 ( $\simeq 13\%$ ) (Bissaldi et al. 2011). This implies that the fraction of bursts with the spectral type (ii) is small, and thus we might not require significant fine tuning of parameters for general GRBs.<sup>12</sup>

We have focused on baryonic jets which evolve roughly adiabatically and have applied a simple analytical formulation of the radiation from the photosphere and internal shock to deduce the physical parameters of the jets for each time-bin. The fine tunings of several parameters appear to be required for the three bursts we have studied, which might suggest other possibilities, e.g., non-adiabatic (i.e., significantly dissipative) jets (Rees & Mészáros 2005), or magnetically-dominated jets (e.g., Thompson 1994; Spruit et al. 2001; Lyutikov 2006; Giannios 2006; Fan 2009; Zhang & Yan 2011). Even in those other jet models, however, the photospheric emission, its up-scattering effect in the internal shocks at large radii,<sup>13</sup> and the change of the radiation properties due to the interaction of the jet with the dense environment could be important for some cases.

<sup>12</sup> The analysis results of the BATSE data ( $\sim 30$  keV – 2 MeV) show that many spectra are adequately fitted with a cutoff power-law function as well as a Band function (Kaneko et al. 2006), so that they are not suitable for constraining the  $\beta$  values and our model.

<sup>13</sup> Even in the jets in which the magnetic field energy is dominant at the base of the jet, the field energy can be converted into the kinetic energy through the jet expansion, leading to the internal shocks at large radius (e.g., Granot et al. 2011).

Thus, the time-binned spectra and delay timescales of the LAT emission onsets could have the potential of revealing the radial structure of GRB jets. The difference in the delay timescales of long and short GRBs may provide clues for understanding the differences between the jets themselves as well as their progenitors.

## ACKNOWLEDGMENTS

We thank the *Fermi* LAT/GBM group members, B. B. Zhang, and T. Sakamoto for useful discussions. We also thank the anonymous referee for comments that significantly improved the paper. We acknowledge NASA NNX09AT72G, NASA NNX08AL40G, and NSF PHY-0757155 for partial support. XFW was supported by the National Natural Science Foundation of China (grants 10633040 and 10921063), National Basic Research Program of China (973 Program 2009CB824800), and the Special Foundation for the Authors of National Excellent Doctorial Dissertations of P. R. China by Chinese Academy of Sciences. PM is grateful for the hospitality of the Institute for Advanced Study, Princeton, during part of this project.

## REFERENCES

- Abdo, A. A., et al. 2009a, *ApJ*, 707, 580  
 Abdo, A. A., et al. 2009b, *Science*, 323, 1688  
 Abdo, A. A., et al. 2009c, *ApJ*, 706, L138  
 Abdo, A. A., et al. 2010, *ApJ*, 712, 558  
 Abramowicz, M. A., Novikov, I. D., & Paczynski, B. 1991, *ApJ*, 369, 175  
 Ackermann, M., et al. 2010a, *ApJ*, 716, 1178  
 Ackermann, M., et al. 2010b, *ApJ*, 717, L127  
 Ackermann, M., et al. 2011, *ApJ* in press (arXiv:1101.2082)  
 Asano, K., Guiriec, S., & Mészáros, P. 2009a, *ApJ*, 705, L191  
 Asano, K., Inoue, S., & Mészáros, P. 2009b, *ApJ*, 699, 953  
 Asano, K., & Terasawa, T. 2009, *ApJ*, 705, 1714  
 Band, D. L., et al. 1993, *ApJ*, 413, 281  
 Beloborodov, A. M. 2005, *ApJ*, 618, L13  
 Beloborodov, A. M. 2010 *MNRAS*, 407, 1033  
 Bissaldi, E., et al. 2011, submitted (arXiv:1101.3325)  
 Böttcher, M., & Dermer, C. D. 1998, *ApJ*, 499, L131  
 Briggs, M. S., et al. 1999, *ApJ*, 524, 82  
 Brunetti, G. 2000, *Astropart. Phys.*, 13, 107  
 Cenko, S. B., et al. 2010, submitted (arXiv:1004.2900)  
 Corsi, A., Guetta, D., & Piro, L. 2010, *ApJ* 720, 1008  
 Daigne, F., Bosnjak, Z., & Dubus, G. 2011, *A&A*, 526, 110  
 Daigne, F., & Mochkovitch, R. 1998, *MNRAS*, 296, 275  
 Dermer, C., & Schlickeiser, R. 1993, *ApJ*, 416, 458  
 De Pasquale, M., et al. 2010, *ApJ*, 709, L146  
 Derishev, E. V., Kocharovskiy, V. V., & Kocharovskiy, V. V. 2001, *A&A*, 372, 1071  
 Eichler, D., & Levinson, A. 2000, *ApJ*, 529, 146  
 Fan, Y. Z., Piran, T., Narayan, R., & Wei, D. M. 2008, *MNRAS*, 384, 1483  
 Fan, Y. Z. 2009, *MNRAS*, 397, 1539  
 Fan, Y. Z. 2010, *MNRAS*, 403, 483  
 Gao, W. H., Mao, J. R., Xu, D., & Fan, Y. Z. 2009, *ApJ*, 706, L33

- Ghirlanda, G., Celloti, A., & Ghisellini, G. 2002, *A&A*, 393, 409
- Ghirlanda, G., et al. 2005, *MNRAS*, 360, L45
- Ghirlanda, G., Bosnjak, Z., Ghisellini, G., Tavecchio, F., & Firmani, C. 2007, *MNRAS*, 379, 73
- Ghirlanda, G., Nava, L., & Ghisellini, G. 2010, *A&A*, 511, 43
- Ghisellini, G., & Celloti, A. 1999, *ApJ*, 511, L93
- Ghisellini, G., Celloti, A., & Lazzati, D. 2000, *MNRAS*, 313, L1
- Ghisellini, G., & Tavecchio, F. 2009, *MNRAS*, 397, 985
- Ghisellini, G., Ghirlanda G., Nava, L., & Celloti, A. 2010, *MNRAS*, 403, 926
- Giannios, D. 2006, *A&A*, 457, 763
- Goodman, J. 1986, *ApJ*, 308, L47
- Granot, J. 2010, in the proceedings of "The Shocking Universe - Gamma-Ray Bursts and High Energy Shock Phenomena", Venice, September 14-18, 2009 (arXiv:1003.2452)
- Granot, J., Cohen-Tanugi, J., & do Couto e Silva, E. 2008, *ApJ*, 677, 92
- Granot, J., & Guetta, D. 2003, *ApJ*, 2003, 598, L11
- Granot, J., Komissarov, S. S., & Spitkovsky, A. 2011, *MNRAS*, 411, 1323
- Greiner, J., et al. 2009, *A&A*, 498, 89
- Gruzinov, A., & Mészáros, P. 2000, *ApJ*, 539, L21
- He, H.-N., Wu, X.-F., Toma, K., Wang, X.-Y., & Mészáros, P. 2010, submitted (arXiv:1009.4716)
- Ioka, K. 2010, *Prog. Theor. Phys.*, 124, 667
- Ioka, K., Murase, K., Toma, K., Nagataki, S., & Nakamura, T. 2007, *ApJ*, 670, L77
- Kaneko, Y., et al. 2006, *ApJS*, 166, 298
- Kobayashi S., Piran T., & Sari R. 1997, *ApJ*, 490, 92
- Königl, A. 1981, *ApJ*, 243, 700
- Kumar, P., & Barniol Duran, R. 2009, *MNRAS*, 400, L75
- Kumar, P., & Barniol Duran, R. 2010, *MNRAS*, 409, 226
- Kumar, P., & McMahon, E. 2008, *MNRAS*, 384, 33
- Kumar, P., Narayan, R., & Johnson, J. L. 2008, *MNRAS*, 388, 1729
- Lazzati, D., & Begelman, M. C. 2010, 725, 1137
- Lazzati, D., Morsony, B., & Begelman, M. C. 2009, *ApJ*, 700, L47
- Li, Z. 2010, *ApJ*, 709, 525
- Lithwick, Y., & Sari, R. 2001, *ApJ*, 555, 540
- Liu, R.-Y., & Wang, X.-Y. 2010, *ApJ* in press (arXiv:1009.1289)
- Lyutikov, M. 2006, *New Journal of Physics*, 8, 119
- Marscher, A. 2009, in *Lecture Notes in Physics* 794, *The Jet Paradigm- From Microquasars to Quasars*, ed. T. Belloni (arXiv:0909.2576)
- Medvedev, M. V. 2000, *ApJ*, 540, 704
- Mészáros, P. 2006, *Rep. Prog. Phys.*, 69, 2259
- Mészáros, P., Laguna, P., & Rees, M. J. 1993, *ApJ*, 415, 181
- Mészáros, P., & Rees, M. J. 1997, *ApJ*, 476, 232
- Mészáros, P., & Rees, M. J. 2000, *ApJ*, 530, 292
- Mizuta, A., Nagataki, S., & Aoi, J. 2010, submitted (arXiv:1006.2440)
- Morsony, B. J., Lazzati, D., & Begelman, M. C. 2007, *ApJ*, 665, 569
- Morsony, B. J., Lazzati, D., & Begelman, M. C. 2010, *ApJ*, 723, 267
- Murase, K., Toma, K., Yamazaki, R., Nagataki, S., & Ioka, K. 2010a, *MNRAS*, 402, L54
- Murase, K., Toma, K., Yamazaki, R., & Mészáros, P. 2010b, submitted (arXiv:1011.0988)
- Nakar, E., Piran, T., & Sari, R. 2005, *ApJ*, 635, 516
- Paczynski, B. 1986, *ApJ*, 308, L43
- Paczynski, B. 1990, *ApJ*, 363, 218
- Panaitescu A., & Kumar P. 2002, *ApJ*, 571, 779
- Panaitescu, A., & Mészáros, P. 2000, *ApJ*, 544, L17
- Pe'er, A., Mészáros, P., & Rees, M. J. 2005, *ApJ*, 635, 476
- Pe'er, A., Zhang, B. B., Ryde, F., et al. 2010, submitted (arXiv:1007.2228)
- Pe'er, A., & Waxman, E. 2004, *ApJ*, 603, L1
- Pe'er, A., & Zhang, B. 2006, *ApJ*, 653, 454
- Piran, T. 2004, *Rev. Mod. Phys.*, 76, 1143
- Preece, R. D., et al. 2000, *ApJS*, 126, 19
- Racusin, J. L., et al. 2008, *Nature*, 455, 183
- Razzaque, S., Dermer, C., & Finke, J. D. 2010, *Open Astronomy Journal*, 3, 150
- Rees, M. J., & Mészáros, P. 1994, *ApJ*, 430, L93
- Rees, M. J., & Mészáros, P. 2005, *ApJ*, 628, 847
- Rosswog, S. 2007, *MNRAS*, 376, L48
- Ryde, F., et al. 2006, *ApJ*, 652, 1400
- Ryde, F., et al. 2010, *ApJ*, 709, L172
- Sari, R., & Esin, A. A. 2001, *ApJ*, 548, 787
- Sekiguchi, Y., & Shibata, M. 2010, submitted (arXiv:1009.5303)
- Shemi, A., & Piran, T. 1990, *ApJ*, 365, L55
- Sikola, M., Begelman, M. C., & Rees, M. J. 1994, *ApJ*, 421, 153
- Spruit, H. C., Daigne, F., & Drenkhahn, G., 2001, *A&A*, 369, 694
- Thompson, C. 1994, *MNRAS*, 270, 480
- Thompson, C., Mészáros, P., & Rees, M. J. 2007, *ApJ*, 666, 1012
- Toma, K., Sakamoto, T., Zhang, B., et al. 2009a, *ApJ*, 698, 1042
- Toma, K., Wu, X. F., & Mészáros, P. 2009b, *ApJ*, 707, 1404
- Vietri, M. 1997, *Phys. Rev. Lett.*, 78, 4328
- Wang, X. Y., & Mészáros, P. 2006, *ApJ*, 643, L95
- Wang, X. Y., Li, Z., Dai, Z. G., & Mészáros, P. 2009, *ApJ*, 698, L98
- Yonetoku, D., et al. 2004, *ApJ*, 609, 935
- Zhang, B. 2007, *Chin. J. Astron. Astrophys.*, 7, 1
- Zhang, B., & Pe'er, A. 2009, *ApJ*, 700, L65
- Zhang, B., & Yan, H. 2011, *ApJ*, 720, 90
- Zhang, B. B., et al. 2010, *ApJ* in press (arXiv:1009.3338)
- Zou, Y.-C., Fan, Y.-Z., & Piran, T. 2011, *ApJ*, 726, L2

This paper has been typeset from a  $\text{\LaTeX}$  file prepared by the author.